Hyperspectral Satellites, Evolution, and Development History

Shen-En Qian , *Senior Member, IEEE*

Abstract—Hyperspectral imaging has been emerged as a new generation of technology for earth observation and space exploration since the beginning of this millennium and widely used in various disciplinary and applications. The fascinating detailed spectral information acquired by hyperspectral imagers often yields results not possible with multispectral or other types of satellites. This article provides an overview of spaceborne hyperspectral imagers, technology evolution, and development history. After introduction of hyperspectral satellites, it first describes the principle of hyperspectral imaging. It then reviews the history of hyperspectral technology development, starting from the first airborne hyperspectral imager AIS built in early 1980s, the first operational airborne hyperspectral imager AVIRIS developed since middle 1980s, the first commercial airborne hyperspectral instrument CASI fabricated since late 1980s, followed by the development of hyperspectral technology in Canada between 1980s and 1990s, and the NASA planned orbiting hyperspectral imagers in 1990s, until the first spaceborne hyperspectral imager Hyperion launched in 2000. This article summarizes the survey carried out by the author on spaceborne hyperspectral imagers to date. There exist at least 25 hyperspectral imagers that have been deployed into space. Among them, 19 are aboard satellites orbiting earth. Six of them are out of earth orbits for Moon, Mars, Venus, and comet missions. The article briefly describes these spaceborne hyperspectral imagers and their mission objectives with the focus on the instrument performance parameters and technical features. This article also briefly reviews six upcoming spaceborne hyperspectral imagers, including EnMAP, MAJIS, OCI, HyspIRI, FLORIS, and CHIME.

Index Terms—Development history, earth observation, hyperspectral satellites, imaging spectroscopy, review, space exploration.

NOMENCLATURE

AaSI	Aalto-1 Spectral Imager.
AHSI	Advanced Hyperspectral Imager on GaoFen-5 satellite.
ARTEMIS	Advanced Responsive Tactically Effective Military Imaging Spectrometer.
CHIME	Copernicus Hyperspectral Imaging Mission for the Environment.
CRISM	Compact Reconnaissance Imaging Spectrometer for Mars on Mars Reconnaissance Orbiter (MRO).
CHRIS	Compact High-Resolution Imaging Spectrometer.
DESIS	DLR Earth Sensing Imaging Spectrometer.
EnMAP	Environmental Mapping and Analysis Program.
FLORIS	Fluorescence Imaging Spectrometer, onboard ESA FLuorescence Explorer (FLEX) mission.
FTHSI	Fourier Transform Hyperspectral Imager on HJ-1A satellite.
HICO	Hyperspectral Imager for Coastal Ocean.
HISUI	Hyperspectral Image Suite.
HSI	HyperSpectral Imager; LEWIS mission.
Hyperion	Hyperspectral Imager.
EO-1	Earth Observing-1 Mission.
HyperScout:	A miniaturized hyperspectral imager with a volume of 1U (10 cm × 10 cm × 10 cm).
HySI	Hyperspectral Imager (HySI) onboard Indian Mini Satellite-1 (IMS-1).
HyspIRI	Hyperspectral Infrared Imager.
M3	Moon Mineralogy Mapper.
MAJIS	Moons and Jupiter Imaging Spectrometer onboard spacecraft of JUpiter ICy moons Explorer.
MERIS	Medium-Resolution Imaging Spectrometer.
ENVISAT	ESA's Environmental Satellite.
MHRIS	Miniature High-Resolution Imaging Spectrometer.
MODIS	Moderate Resolution Imaging Spectroradiometer.
OCI	Ocean Color Instrument.
OLCI	Ocean and Land Color Imager.
PRISMA	PRecursore IperSpettrale della Missione Applicativa.
SPIMs 1-5	Spectrographic Imagers 1-5.
MSX	Midcourse space experiment satellite.
VIRTIS	Visible and Infrared Thermal Imaging Spectrometer.
VNIS	Visible and Near-Infrared Imaging Spectrometer aboard Chang'E 3 Spacecraft.

I. INTRODUCTION

WHILE multispectral satellites, such as Landsat and SPOT satellites, have been in regular use since the 1970s, hyperspectral satellites are emerged as a new generation of remote sensing satellites since the beginning of this millennium. Imaging spectrometry, also known as hyperspectral imaging, is a combination of the traditional spectroscopy technology with the modern imaging system [82].

Spectroscopy technology or spectrometry deals with the measurement of a specific spectrum for identification of matters. It is a key analytical method used to investigate material composition and related processes through the study of the interaction of light with matter. The energy is absorbed by the matter, creating an excited state. The interaction creates some form of electromagnetic waves. By using a spectrometer, one can determine the level of excitement in the matter's atoms to determine what kind of material it is. Determining composition remotely, without physical contact, is one of the most valuable capabilities of spectroscopy. Spectroscopy technology is widely used in laboratories in the disciplines of physics, chemistry, and biology to investigate material properties. Spectroscopic data are often represented by an emission spectrum, a plot of the response of interest as a function of wavelength or frequency. For example, the use of colorimetry for the investigation of cholesterol or blood sugar in chemical laboratories is a form of spectroscopy. Spectrometry has also been used for determining blood alcohol levels, checking automobile emissions, and monitoring smokestack pollution.

An imaging system converts the visual characteristics of an object, such as a physical scene or the interior structure of an object, into digital signals and creates digitally encoded representations that are processed by a processor or computer and made output as a digital image. Imaging systems typically consist of a camera, imaging lens, along with an illumination source. Depending on the system setup, an imaging system can allow observed objects to be magnified or enhanced to ease the viewing or inspection of small or unclear objects. Computers are becoming more and more powerful with increasing capacities for running programs of any kind especially digital imaging software.

The combination of the spectroscopy technology and the modern imaging system is referred to as imaging spectrometry, now also called hyperspectral imaging. It could measure a spectrum for every element (or pixel) in an image. This provides a revolutionary way of observing the earth and other planets by collecting information of each pixel in the field of view across the electromagnetic spectrum. A hyperspectral imager operating in the solar reflected spectrum senses objects in the field of view in detail spectrally and spatially. Molecules and particles of the land, water, and atmosphere environments interact with solar energy in the 400–2500 nm spectral region through absorption, reflection, and scattering processes. These spectral measurements are used to determine constituent composition through the physics and chemistry of spectroscopy for scientific research and applications over the regional scale of the image. The main advantage to hyperspectral imaging is that, because an entire spectrum is acquired for each pixel of the acquired imagery, an operator needs no prior knowledge of the sample, and postprocessing allows all available information from the dataset to be exploited [11]. Hyperspectral imaging can also take advantage of the spatial relationships among the different spectra in a neighborhood, allowing more elaborate spectral-spatial models for a more accurate segmentation and classification of the image [33].

Fig. 1 illustrates the concept and principle of a hyperspectral satellite. It acquires images of a ground scene in hundreds of
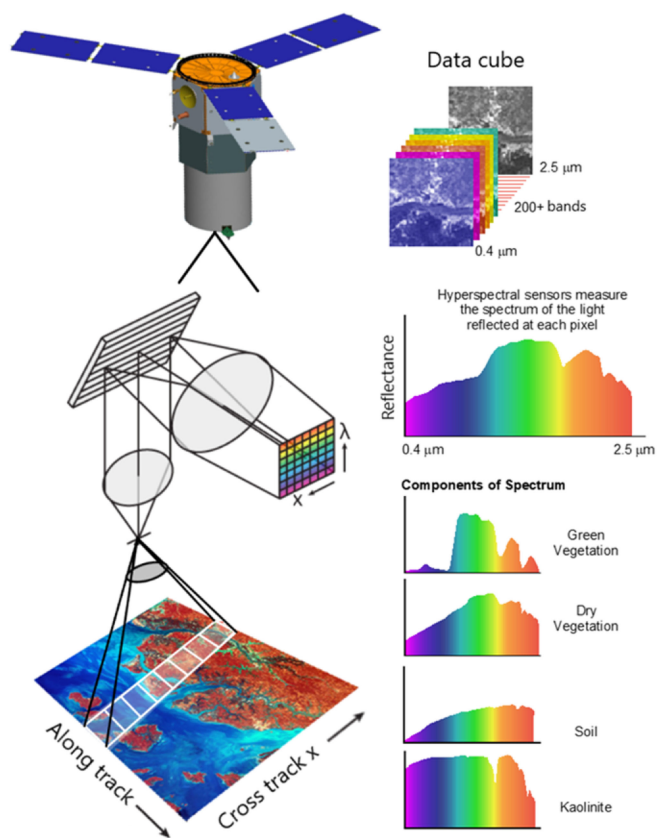

Fig. 1. Illustration of concept and principle of a hyperspectral satellite. A data cube and a spectrum for each pixel are generated by a hyperspectral satellite.

continuous and narrow spectral bands over wavelengths ranging from the near-ultraviolet (UV) to the short wave infrared (SWIR). Each image, often referred to as spectral image or band image, corresponds to a particular wavelength. The collected "data cube" contains both spatial and spectral information of the materials within the scene. Each pixel in the scene is sampled across hundreds of narrow-band images at a particular spatial location in the data cube, resulting in a one-dimensional (1-D) spectrum. It is a plot of wavelength versus radiance or reflectance. The spectrum for a single pixel acquired by a hyperspectral satellite appears similar like a spectrum collected by a spectrometer in a spectroscopy laboratory. The spectrum can be used to identify and characterize the particular feature of the pixels within the scene based on the unique spectral signatures or "fingerprints." Hyperspectral imagery can provide direct identification of the surface materials and has been used in a wide range of remote sensing applications, including geology, agriculture, forestry, environment, ocean, atmosphere, climate change, defence and security, and law enforcement. The fascinating detailed spectral information provided by hyperspectral imagery often yields results not possible with multispectral or other types of imagery [83].

II. HYPERSPECTRAL IMAGING APPROACHES

Hyperspectral imagers acquire both spatial and spectral information of a scene and generate a data cube for the scene. There are at least four different approaches to acquiring (?) the

hyperspectral imagery in terms of the spectral dispersion means, or type of imaging spectrometers used.

1) Dispersive elements based approach.
2) Spectral filters based approach.
3) Fourier transform imaging interferometer.
4) Snapshot hyperspectral imaging.

This article reviews these approaches.

A. Dispersive Elements Based Approach

A dispersive element based hyperspectral imager separates the radiation light from an object into spectral components using dispersive elements, such as prisms or diffraction gratings. A grating or a transparent prism is inserted into the collimated beam of the spectrometer to break radiation light up into its constituent monochromatic components. The monochromatic components dispersed by a grating are in linear distribution, whereas the monochromatic components dispersed by a prism are in nonlinear distribution. A grism can also be used to break radiation light up into its constituent monochromatic components. A grism is a combination of a grating and prism (also called a grating prism) so that radiance light at a chosen central wavelength passes straight through.

Dispersive element based hyperspectral imagers are the most popular ones for both airborne and spaceborne remote sensing. This type of hyperspectral imagers needs to scan the scene on ground either by a dedicated scanner or by the entire instrument with the aircraft or satellite flight motion to obtain the spatial coverage. There are two operating modes in terms of scanning of the scene: whiskbroom and pushbroom. A dispersive element based hyperspectral imager that uses 1-D linear detector arrays operates in whiskbroom mode, whereas a dispersive element based hyperspectral imager that uses 2-D area detector arrays operates in pushbroom mode.

For the early airborne hyperspectral imagers, whiskbroom operating mode was often used, such as the airborne visible/infrared imaging spectrometer (AVIRIS) developed by NASA's Jet Propulsion Laboratory (JPL) [41]. This was because 1-D linear detector arrays were used that could record the monochromatic components of the spectrum of only one ground pixel (or ground sampling cell) at a moment. The instrument needs to scan the ground sampling cells one after another in a cross-track line using the whiskbroom mode as shown in Fig. 2. After completion of scanning all the ground sampling cells in the current cross-track line, the instrument starts to scan the ground sampling cells of the next cross-track line when the aircraft or satellite flies forward in the flight direction (also referred to as along-track direction), and so on.

The advantages of a whiskbroom hyperspectral imager are as follows.

1) Simple design of the instrument.
2) Wide swath (i.e., the length of the cross-track line), as the swath width is determined by the scanning mechanism rather than by the available number of pixels in the spatial direction of the 2-D detector array.
3) Easy calibration, since all the spectra of the ground sampling cells within the scene are generated by the same
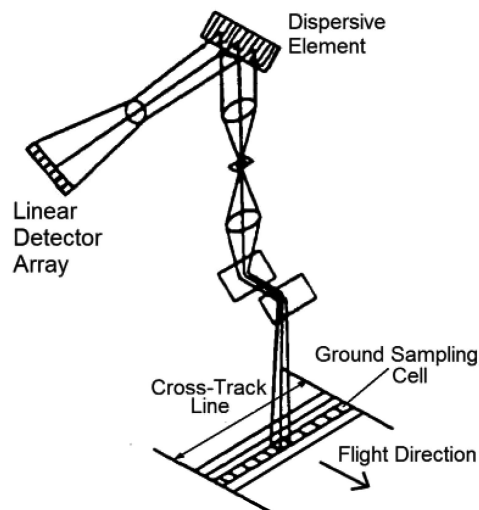

Fig. 2. Concept of a hyperspectral imager operating in whiskbroom mode using a linear detector array.

linear detector array and the same optics, which have the identical spectral characteristics. This type of hyperspectral imager has no spatial distortion (also referred to as keystone) as does of a pushbroom hyperspectral imager.

The disadvantages of a whiskbroom hyperspectral imager are as follows.

1) A mechanical scanner is required, which contains moving parts in vacuum chamber.
2) Postprocessing is required for spatial incongruence.
3) Constraints of high spectral and spatial resolution requirements due to low integration time.

Almost all the spaceborne hyperspectral imagers use 2-D area detector arrays and operate in pushbroom operating mode. Fig. 3 shows an example of the concept of a dispersive element based hyperspectral imager that uses a 2-D detector array. As shown in the figure, it images an entire line of ground sampling cells in the cross-track direction, whereas an aircraft or spacecraft provides the forward scan in along-track direction. No scanning of individual ground sampling cell one after another is required. The 1-D image of the cross-track line, formed on the spectrometer slit, is then dispersed onto the 2-D detector array, which provides spectral information along one axis and spatial information along the other. This architecture effectively integrates as many individual spectrometers as there are ground sampling cells in the cross-track line into a single instrument.

The advantages of a dispersive element based hyperspectral imager that operates in the pushbroom mode are as follows.

1) No moving parts.
2) Congruence spatial images.
3) Longer integration time for each ground sampling cell, because each of them is sensed simultaneously by a row elements of the 2-D detector array (e.g., rows A, B, C, ..., G in Fig. 3) instead of one after another, which omits the time sharing scanning of all the ground sampling cells in a cross-track line. Longer integration time means more photos are collected and results in higher signal-to-noise ratio (SNR).
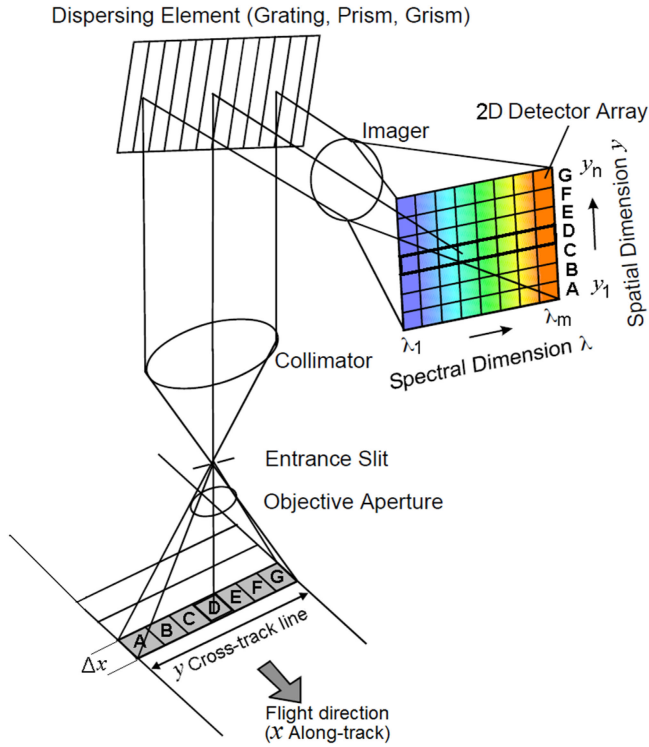
Fig. 3.   Example of the concept of a dispersive elements based hyperspectral imager.

Fig. 4.   LVF and its spectral passbands.

The disadvantages of a pushbroom hyperspectral imager are as follows.

1) Complex optical design and complex focal plane.
2) Swath width is constrained by the available number of pixels of the 2-D detector array in the spatial direction.
3) Complex calibration.
4) There are both spectral distortion (also referred to as smile) and spatial distortion (also referred to as keystone). The hyperspectral data collected by a pushbroom hyperspectral imager need to be sufficiently corrected for smile and keystone distortion before being distributing to users for downstream applications [82].

B. Spectral Filters Based Approach

Spectral filters based hyperspectral imagers are less popular and appear more recently. One or more spectral filters, such as an absorption or interference filter, are used to transmit the selected spectral bands of interest. As the beam passes through a filter, some of its spectral components are blocked through an absorption or interference process, whereas the desired spectral components are transmitted. Various absorption or interference filters, from the UV through the far-infrared region in various dimensions are available as commercial-off-the-shelf (COTS) products. An electronically tunable filter (ETF) is another kind of spectral filter that transmits desired spectral bands by controlling voltage, or acoustic signal, etc. [27].

The basic principle of a spectral filter based hyperspectral imager is similar to a dispersive element-based imager. However, the main difference is that the ra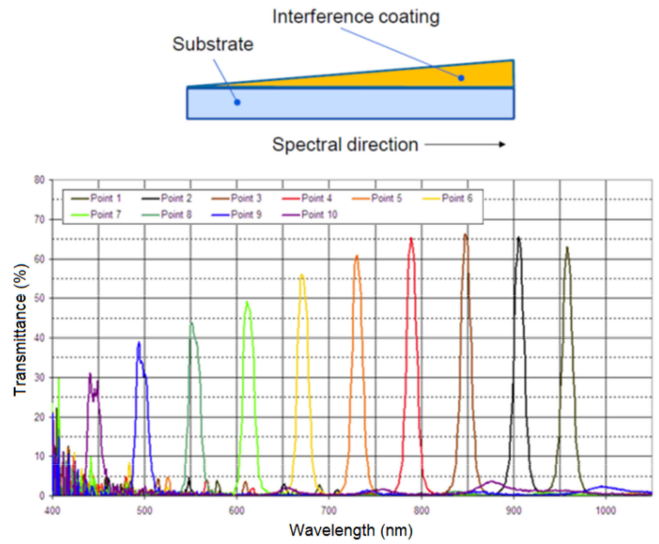diation light from a telescope is directly focused on a 2-D filter, instead of being collimated and then dispersed by a grating or prism in a traditional spectrometer. The filter has the same size as the 2-D detector array and is assembled close to the detector's sensitive surface. It distributes spectral content of the ground sampling cells in the spectral dimension.

An example of spectral filter is an optical wedge filter, also referred as to a linear variable filter (LVF). It is a glass coated with an interference filter of increasing thickness along one direction. This direction is called as the spectral direction. The passband, i.e., spectral position of the peak of the transmission curve, varies with the thickness of the deposition, as shown in Fig. 4. Hence, the spectral passband varies linearly along one physical dimension of the filter.

Fig. 5 illustrates the concept of an LVF-based hyperspectral imager. A simple pushbroom hyperspectral imager can be built by placing an LVF in front of a 2-D detector array after the telescope collects the input radiation light of a ground scene. The 2-D detector array of the instrument "sees" the complete scene at once. Recall that described in Section II-A, a dispersive element based hyperspectral imager working in pushbroom mode acquires an entire cross-track line on ground at a moment (see Fig. 3), whereas a dispersive element based hyperspectral imager working in whiskbroom mode acquires a single ground sampling cell in a cross-track line at a moment (see Fig. 2). Unlike a dispersive element based hyperspectral imager, an LVF-based hyperspectral imager acquires simultaneously all the cross-track lines in the field-of-view (FOV), this is because the FOV of an LVF-based hyperspectral imager is not limited to only one cross-track line by a slit in the along-track direction. Each row of the 2-D detector array images a corresponding cross-track line of the FOV but in a different waveband than the neighboring lines. Hence, at every moment of time a detector frame is imaged, a complete 2-D scene is acquired. Each line of the scene is acquired at a different wavelength. As the satellite flies over the scene, each filter row passes over the scene. Once the complete
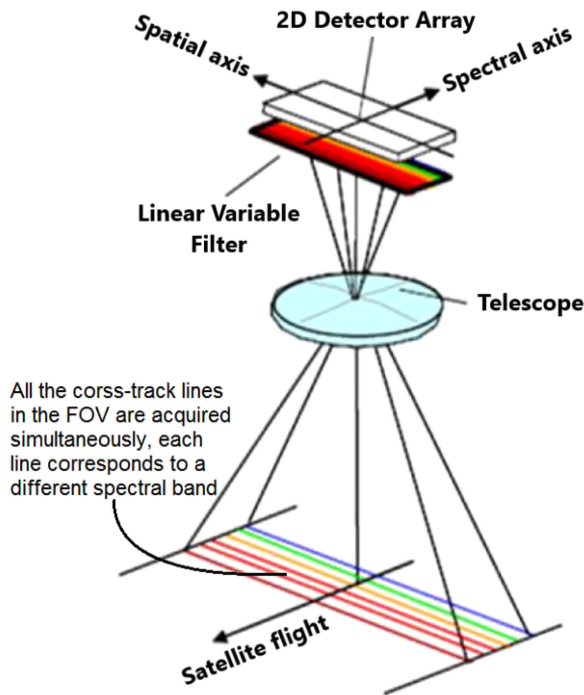
Fig. 5.   Illustration of the concept of an LVF-based hyperspectral imager.

Fig. 6.   OCSF (each step having six rows with the same spectral bandpass filters) and two OCSF-based hyperspectral cameras.

FOV has passed over the sense, each different filter row sensed all cross-track lines of ground sampling cells in the scene and acquired all spectral components. A full spectrum curve of each ground sampling cell can be reconstructed by reorganizing these images acquired at different moments.

There are at least two spaceborne hyperspectral imagers that use an LVF to disperse the spectrum of radiation light. The Hyperspectral Imager (HySI) onboard Indian Mini Satellite-1 (IMS-1) launched in April 2018 used an LVF, which covers a wavelength range from 400 to 950 nm dispersed over 512 spectral elements of the detector array. This resulted in an oversampling at about 1 nm spectral sampling interval (SSI). Considering the application requirements and the limitations of data rate, 8 band binning was incorporated. After binning, the spectral bandwidth becomes 8 nm with a total of 64 spectral bands [53]. Another LVF-based spaceborne hyperspectral imager is hyperspectral nanosatellite HyperScout. It is a 3U CubeSat with the hyperspectral imager being 1U (10 cm × 10 cm × 10 cm). The LVF covers a wavelength range from 450 to 900 nm with an SSI of 10 nm [16].

Fabry–Pérot interferometer (FPI) based filters have been adopted to transmit the selected spectral bands of interest. A Fabry–Pérot filter allows some wavelengths to pass, whereas others are filtered out. Its transmission spectrum as a function of wavelength exhibits peaks of large transmission corresponding to resonances of the etalon. By carefully controlling the distance between the reflecting mirror surfaces, a Fabry–Pérot filter can be designed to transmit only a narrow-wavelength band wanted. Geelen *et al.* [34] reported that Fabry–Pérot filters in a wavelength range of visible and near infrared (VNIR) (400–1000 nm) have been made in traditional semiconductor fabrication process and directly integrated on top of a wafer that
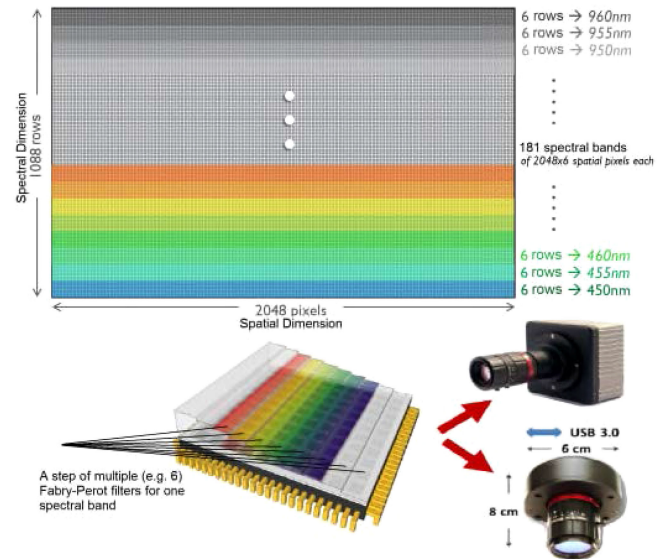
contains silicon-based CMOS image sensor chips. The use of monolithically integrated Fabry–Pérot filters on top of a detector array is an innovative approach to combining spectroscopy with imaging technology for hyperspectral imagers. This can result in low cost, compactness, and high speed. As a natural evolution of this innovative technology, the wavelength range of the CMOS-based Fabry–Pérot filters has been extended to the SWIR: 1000–1700 nm, together with InGaAs-based detector arrays [47].

This new integration approach is unique and has attractive advantages: First, combining the production of filters and detector arrays into one CMOS-compatible process leads to an overall simplification and cost reduction, and enables massive production. Second, the monolithic integration induces less cross-talk between neighboring bands and reduces stray light in the system. This also has a positive effect on the system's sensitivity and speed. The upper part of Fig. 6 shows a silicon-based CMOS detector array of size 1088 rows by 2014 pixels working in a wavelength range of VNIR. The same size bandpass Fabry–Pérot filters are integrated on top of the pixels in a particular row of the detector array when the detector array was fabricated at the wafer level. The spectral bandpass of the filters is controlled by the distance between the two parallel mirror surfaces (i.e., the thickness). The same bandpass Fabry–Pérot filters can be deployed on multiple rows of the detector array. In the figure, the same bandpass filters (having the same thickness) are integrated on top of every six adjacent rows of pixels. These multiple rows of pixels have the same thickness (or height) of deposited filters and look like a step of a stair. This is why, this kind of Fabry–Pérot filter on top of a detector array is also referred to as on-chip stepped filters (OCSF), as illustrated at the lower part in Fig. 6.

The configuration of the OCSF is a series of filter rows disposed of one behind each other in the along-track direction that allows to create a pushbroom hyperspectral imager as same as an LVF-based hyperspectral imager. Most importantly, this

configuration provides the choice to sense objects on ground using multiple detector rows (such as six rows) of the same spectral bandpass to boost the SNR using the on-chip time delayed integration or off-chip data binning in spectral dimension. The VNIR detector array with the OCSF shown in Fig. 6 has 181 spectral bands spanning a wavelength range from 450 to 960 nm with an SSI of 5 nm. The full-width at half-maximum (FWHM) of each spectral band is about 15 nm. The width of a step is six detector rows (these rows are deposited the same Fabry–Pérot filters).

Lower part of Fig. 6 shows two COTS hyperspectral cameras that were fabricated by the IMEC using an OCSF. They consist of a fore-optics and a silicon-based CMOS detector array with integrated OCSF, plus imaging controlling electronics. There are no spectrometers in the hyperspectral cameras. That is why their volume and mass are all small. The round camera uses IMEC's first generation OCSF covering a spectral range of 600–1000 nm with about 100 spectral bands and 5 nm bandwidth. Its volume is about 6 cm × 6 cm × 8 cm. The mass is around 0.6 kg. The squared camera uses IMEC's second-generation OCSF covering a spectral range of 470–960 nm with about 150 spectral bands.

An ETF-based hyperspectral imager uses a filter that is mounted in front of a monochrome camera by electronically tuning its spectral transmission (i.e., bandpass) to produce a stack of image slices at a sequence of wavelengths. An ETF is a device whose spectral transmission can be electronically controlled by applying voltage, acoustic signal, etc. [27]. The advantage of an ETF-based hyperspectral imager is that an entire 2-D spatial image of a spectral band is formed instantly when the filter tunes to a particular bandpass wavelength. Unlike dispersive element based and LVF/OCSF-based hyperspectral imagers, there is no need to observe multiple cross-track lines by the satellite flight motion to obtain the second spatial dimension or to accumulate the spectral dimension. This advantage is at the cost of the additional time required to tune the ETF to cover the whole wavelength range before the satellite moves its FOV to observe the next scene on the ground.

There are typically following three categories of ETFs.
1) Liquid crystal tunable filter (LCTF).
2) Acoustooptic tunable filter (AOTF).
3) Interferometer-based filters.

An LCTF uses electronically controlled liquid crystal elements to transmit a desired wavelength of light and block others. It has advantages of high image quality and relatively easy to be integrated into an optical system. Its disadvantage is lower peak transmission values in comparison with conventional fixed-wavelength optical filters due to the use of multiple polarizing elements. An AOTF is based on the principle of diffraction. An acoustooptic modulator, also called a Bragg cell, uses the acoustooptic effect to diffract and shift the frequency of light. Compared with an LCTF, an AOTF has a faster tuning speed (microseconds versus milliseconds) and a wider wavelength range. Its disadvantage is relatively poor imaging quality due to the acoustooptic effect of sound waves to diffract and shift the frequency of light.

Abdlaty *et al.* [1] compared performance between an AOTF-based and LCTF-based hyperspectral imager in medical applications for the purpose of highlighting the leverage points of the
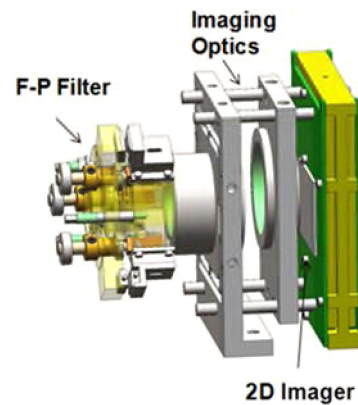

Fig. 7. Concept drawing of an electronically tunable Fabry–Pérot filter based hyperspectral imager.

two types of filters to facilitate their selection in hyperspectral imager design. In their experiments, three parameters were examined: spectral resolution, out-of-band suppression (i.e., spectral cross-talk), and image quality in the sense of spatial resolution. The experimental results demonstrated that AOTF-based hyperspectral imager showed superiority in spectral resolution, out-of-band suppression, and random switching speed between wavelengths, whereas LCTF-based hyperspectral imager had better performance in terms of the spatial image resolution, both horizontal and vertical, and high definition quality. They concluded that an efficient design of a hyperspectral imager is application-dependent. For medical applications, for instance, if the tissue of interest required more spectral information for undefined optical properties, or contains close spectral features, AOTF might be the better option. Otherwise, LCTF is more convenient and simpler to use, especially if the tissue chromophore's spatial mapping is needed.

The Visible and Near-Infrared Imaging Spectrometer (VNIS) aboard Chinese Chang'E-3 lunar spacecraft is an AOTF-based hyperspectral imager [97]. Chang'E 3 achieved lunar orbit on December 6, 2013 and soft-landed on the Moon on December 14, 2013.

A Fabry–Pérot filter is an interferometer-based filter. Fig. 7 shows a concept drawing of a Fabry–Pérot filter based hyperspectral imager. The Fabry–Pérot filter is mounted in front of the imaging optics and let pass only light that is at the resonance condition $\lambda = 2d$ (first-order). Each plate separation generates a 2-D image at a wavelength with spectral extent given by the FWHM of the transmission response. The way of a Fabry–Pérot filter used here is different from that in the on-chip Fabry–Pérot filter (OCFPF) based hyperspectral imager. Fabry–Pérot filters used here are tunable for bandpass by electronically controlling the width of the cavity, whereas Fabry–Pérot filters used in on-chip filters are deposited on top of a CMOS detector array at wafer fabrication level with the fixed cavity for a fixed bandpass.

There are at least two spaceborne hyperspectral imagers that are based on the technology of electronically tunable Fabry–Pérot filters. The Greenhouse Gas Satellite - Demonstrator (GHGSat-D) microsatellite mission, which was launched in June 2016 [35], uses an electronically tunable Fabry–Pérot filter operating in a wavelength region between 1600 and 1700 nm
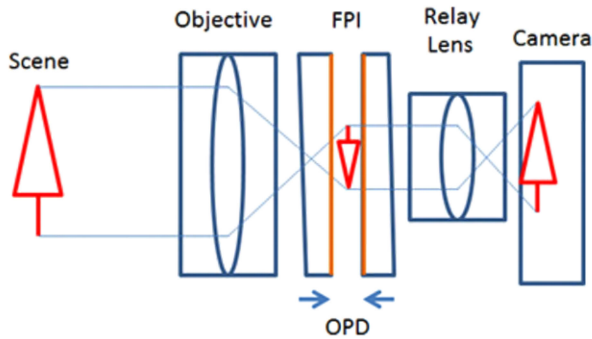
Fig. 8. Scheme of hyperspectral imager based on an FPI [101].

Fig. 9. Scheme of a Fourier transform hyperspectral imager using a spatially modulated imaging interferometer.

with a spectral resolution on the order of 0.1 nm. This wavelength range and spectral resolution were selected for the presence of spectral features for greenhouse gases methane and carbon dioxide, as well as relatively little interference from other atmospheric species, H_2O in particular. This miniaturized ETF-based hyperspectral imager has a mass of 5.4 kg and a volume of 36 cm $\times$ 26 cm $\times$ 180 cm. Another spaceborne hyperspectral imager that uses a tunable Fabry–Pérot filter is Aalto-1 Spectral Imager (AaSI) onboard the Aalto-1 3U CubeSat launched in June 2017. The Fabry–Pérot filter is electronically controlled in a closed capacitive feedback loop by three different piezo actuators to cover a spectral range from 500–900 nm with a spectral resolution of 6–20 nm [80], [81].

C. Fourier Transform Imaging Interferometer

This kind of hyperspectral imagers is based on interferometers [2], where the spectrum for each pixel is obtained by applying Fourier transform based algorithm to the interferogram obtained by scanning the optical path difference (OPD) of the interferometer. This technology has been utilized for decades by spectroscopists to obtain high-resolution absorption spectra using a Michelson interferometer (two beam) or an FPI (multibeam). There are many attractive features that make interferometer-based spectrometers comparable to the conventional dispersive spectrometers. First, the multiplex advantage arises from the fact that there is no spectral scanning and all the spectral components are acquired at the same time. Second, the throughput advantage originates from the fact that the aperture used in Fourier spectrometers has a larger area than the slits used in dispersive spectrometers, thus enabling higher throughput of radiation. These two features combined together make the interferometer-based spectrometer a faster instrument (or equivalently having a higher SNR) with respect to the other spectrometers at the same resolution.

A hyperspectral imager based on an FPI is shown in Fig. 8. An interferometer is placed in the optical system in front of the camera. A scene is first imaged in the FPI so that the transmitted intensity is modulated by the interference, whereas the OPD of the interferometer is varied. The second image is then formed on the detector array of the camera by means of the relay lens. A sequence of frames carrying the interference fringe information is acquired synchronized with the scan of
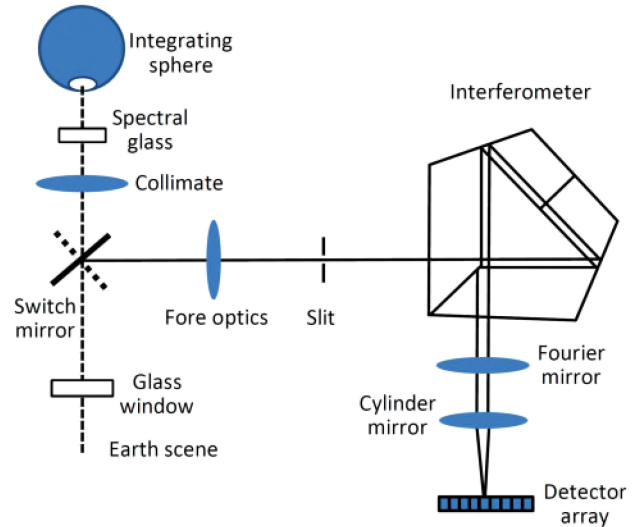
the OPD between the two mirrors of the FPI from contact to the maximal distance of the mirror. The interferogram for each pixel is acquired by the camera and the spectrum is calculated with an algorithm based on the Fourier transform. The final attainable resolution in principle is only limited by the maximal OPD of the interferometer [101].

Hyperspectral imagers based on Michelson interferometers have been implemented with success in commercial instruments with more than 500 spectral bands in the infrared region and reaching a spectral resolution of less than 1 cm^{-1} [9], [49]. Fig. 9 shows the construction diagram of a Fourier transform based hyperspectral imager (FTHSI), a spatially modulated imaging interferometer. It consists of a fore-optics, Fourier interferometer and calibration subsystem. In the fore-optics, a switch mirror is equipped to select the incoming light of the interferometer for observation or calibration. When the mirror is turned to the observation position, the incoming radiation light from a scene on ground is directed toward the interferometer. When the mirror is turned to the calibration position, the incoming light from the calibration subsystem is directed toward the interferometer.

There is at least one FTHSI that has been deployed in space. The Chinese Huan Jing 1A (HJ-1A) satellite carries an FTHSI, which was launched on September 6, 2008. Huan Jing (HJ) in Chinese means environment. HJ minisatellite constellation is a national program led by the National Committee for Disaster Reduction and the State Environmental Protection Administration of China to construct a network of earth observing satellites. The overall objective is to establish an operational earth observing system for disaster monitoring and mitigation using remote sensing technology and to improve the efficiency of disaster mitigation and relief. The FTHSI is based on a spatially modulated imaging interferometer. FTHSI generates a total of 115 bands covering a spectral range from 0.45 to 0.95 μm after processing of the raw Fourier transform data and returning to spectral domain. The data processing and calibration of the FTHSI instrument was reported by Zhao et al. [100].

D. Snapshot Hyperspectral Imagers

Dispersive element-based hyperspectral imagers require a scanning either whiskbroom (point-scanning) or pushbroom (line-scanning) to generate a hyperspectral data cube. Spectral filters based hyperspectral imagers require a wavelength scanning (using spectral filters) to generate a hyperspectral datacube. A snapshot hyperspectral imager generates a hyperspectral data cube in a single integration time of a detector array. No scanning is required. It incorporates specialized components to distribute a scene's 3-D spatial-spectral information onto a 2-D detector array. Snapshot hyperspectral imaging typically requires 2-D detector arrays with a high number of pixels. The elimination of moving parts means that motion artifacts can be avoided.

The design and fabrication of a snapshot hyperspectral imager are generally more complex than those of the scanning hyperspectral imagers. A snapshot hyperspectral imager makes use of recent technology, such as large format detector arrays, high-speed data transmission, advanced optical manufacturing methods, and precision optics. It can often offer much higher light collection efficiency than the equivalent scanning instruments. However, this advantage can be fully benefited only by tailoring the design to particular applications, such as professional astronomical community. One of the main reasons for the popularity of snapshot technology in the astronomical community is that it offers large increases in the light collection capacity of a telescope when performing hyperspectral imaging [43].

There are the following five popular snapshot spectral imaging technologies [44].

1) Multi-aperture filtered camera (MAFC).
2) Coded aperture snapshot spectral imager (CASSI).
3) Image mapping spectrometry (IMS).
4) Snapshot hyperspectral imaging Fourier transform spectrometer (SHIFT).
5) OCFPF.

A MAFC is composed of an array of imaging elements, such as a monolithic lenslet array, with a different filter placed at each element of the detector array to collect a desired spectral band. There are typically three different versions of implementation in terms of the locations of the lenslet array and the spectral filters. In implementation version 1, the lenslet array is placed at the focal plane of the objective lens, and the detector array lies at a pupil plane as imaged by the lenslet array. The image behind each lenslet is an image filtered by the filter array and modulated by the scene's average spectral distribution across the lenslet. This implementation has an advantage of being able to use a variety of objective lenses, so that zooming, refocusing, and changing focal lengths are easier to achieve at the cost of more complex and less compact [46], [55]. In other two implementation versions, the lenslet array is located after the collimating lens with the filter array being either in front of the lenslet array or behind the lenslet array before the spectral components entering the detector array.

Fig. 10 depicts the concept of a MAFC snapshot hyperspectral imager. In this case, the lenslet array is located after the collimating lens with the filter array being at the back of the lenslet array. A 2-D LVF having the same size as the detector array is placed in front of the detector array to separate the input radiation light
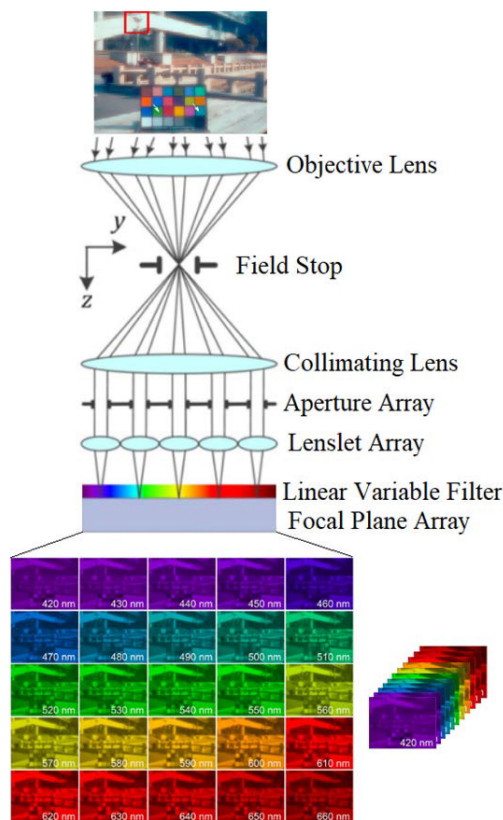

Fig. 10. Illustration of the concept of a snapshot hyperspectral imager.

of a scene into different spectral band images corresponding to the lenslet array. In the figure, a total of 25 different spectral band images of the scene are generated simultaneously. These band images cover a wavelength range from 420 to 660 nm with a spectral bandwidth of 10 nm. By organizing these band images in the order of wavelength, a hyperspectral data cube is formed.

A CASSI is formed by replacing the entrance slit of a dispersive spectrometer with a much wider field stop. A binary coded mask (e.g., an S-matrix pattern or a row-doubled Hadamard matrix) is inserted inside the field stop. The mask creates a transmission pattern at each column within the slit such that each column's transmission code is orthogonal to that of every other column. The encoded light, transmitted by the coded mask within the field stop, then passes through the collimating lens, disperser, lens, and final reaches onto the detector array of a standard spectrometer. Because the columns of the coded mask are orthogonal, when they are smeared together by the disperser and multiplexed on the detector array, they can be demultiplexed during postprocessing [64], [95], [96].

An IMS-based snapshot spectral imager uses an array of microfaceted mirrors placed at an image plane. These mirror facets share the same tilt angle, so that multiple slices of the image are mapped to each individual pupil plane. The resulting pattern imaged at the detector array resembles a scene through a picket fence. If there are p (e.g., $p = 9$) individual pupils in the imager system, then p subimages are generated. Assembling all p subimages, a hyperspectral data cube is obtained. The IMS approach allows each pupil to be shared among many mirror

facets; the system design becomes much more compact and allows for higher spatial resolution.

The first IMS-based snapshot spectral imager (referred to as an image slicing spectrometer at that time) has been reported [25]. The demonstrated prototype can simultaneously acquire 25 spectral band images spanning a spectral range of 140 nm with a spectral bandwidth of 5.6 nm for fluorescence spectroscopy. The generated hyperspectral data cube has a size of 100 pixels $\times$ 100 pixels $\times$ 25 spectral bands using a charge-coupled device (CCD) array. Two years late, the data cube size was increased to $350 \times 350 \times 46$ [26]. The IMS-based snapshot spectral imaging technology has been applied to remote sensing applications, such as monitoring vegetation, urban development, and lightning observation. Dwight *et al.* [23] reported a compact snapshot image mapping spectrometer (SNAP-IMS) for unmanned aerial vehicle (UAV) hyperspectral imaging in collaboration with a NASA team. The SNAP-IMS instrument has a FOV of 10.6° and an instantaneous FOV (IFOV) of 0.03°. It can acquire a hyperspectral data cube of size $350 \times 400 \times 55$ (x, y, λ) within a single camera frame. These 55 spectral bands are acquired simultaneously covering a wavelength range from 470 to 670 nm in the visible spectral region. This wavelength range is limited only by the choice of the detector array, bandpass filter, and dispersion optics. A hyperspectral data cube can be acquired at 1/500–1/100 s, eliminating motion artifacts associated with the platform motion. The instrument has a very small volume of 28.8 cm $\times$ 15.3 cm $\times$ 16.3 cm and a mass of 3.6 kg. It has been integrated with an Octocopter UAV. The payload's power consumption is marginal as there are no mechanical scanning components. The power is dedicated exclusively to CCD frame acquisition. The small volume and mass and low power consumption can offer longer and higher flights at a smaller drone, which is attractive for nanosatellite or microsatellite missions.

A SHIFT performs its spectral measurement in the time domain. It separates spectrum using a Fourier-domain approach without any spectral filters. It is based on a birefringent polarization interferometer behind a lenslet array [51], [52]. The interferometer contains a pair of Nomarski prisms, NP1 and NP2, each of which consisting of two birefringent crystal prisms with wedge angle α. There is also a half-wave plate between NP1 and NP2. An $N \times M$ lenslet array images a scene through the generating polarizer, a pair of Nomarski prisms and the analyzer polarizer. Thus, $N \times M$ subimages are formed on a detector array. Rotating the interferometer by a small angle δ relative to the detector array enables each one of the subimages to be exposed to a different OPD. Therefore, a 3-D interferogram cube can be assembled by sequentially extracting each one of the subimages. Fourier transformation, along the OPD axis of the interferogram cube, enables reconstruction of the 3-D data cube. This prism-based design allows for a reduced volume and an improved robustness to vibration.

An OCFPF-based snapshot hyperspectral imager is reported by the IMEC in Belgium [34]. The key concept is the use of Fabry–Pérot filters that are directly postprocessed at wafer level on top of a CMOS detector array. It is simply composed of the following three parts.

1) A fore-optics (e.g., an objective lens or a telescope) that forms an image of the scene.
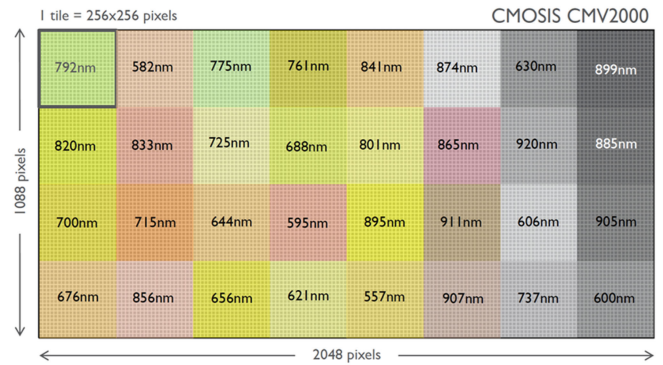

Fig. 11. Fabry–Pérot filters monolithically integrated on top of a CMOS detector array in a tiled configuration for snapshot hyperspectral imaging. Each tile contains 256×256 pixels for a narrow (10–15 nm) band of wavelengths as shown in the tile.

2) An optical subsystem that duplicates the scene onto each filter tile.
3) A filter array organized in a tiled configuration monolithically integrated on top of a CMOS detector array where each filter is designed to sense only one narrow band of wavelengths.

Fig. 11 shows a layout of the Fabry–Pérot filters monolithically integrated on top of a CMOS detector array in a tiled configuration. There are $4 \times 8 = 32$ tiles spanning a wavelength range of 557–920 nm. Each tile contains 256×256 pixels for a narrow (FWHM = $\sim$10–15 nm) band of wavelengths as shown in the tile. These simultaneously acquired spectral bands selected by the filters in the tiles of a scene can be easily reconstructed into a data cube of size $256 \times 256 \times 32$ (x, y, λ). The acquisition speed can be up to 340 data cubes per second.

III. DEVELOPMENT HISTORY OF HYPERSPECTRAL IMAGING TECHNOLOGY—FROM AIRBORNE TO SPACEBORNE IMAGERS

As the sophistication of optical remote sensing instruments and technology development, more applications are being found that require imaging with high spectral resolution. Hyperspectral imagers, which record a full spectrum for each pixel in a scene, are ideal sensors for this purpose. They allow optimal mapping of targets with well-defined spectral signatures for identifying materials in the scene and estimating the effects of atmospheric scattering and absorption, and accurate simulation of the responses of other sensors.

The development of hyperspectral imaging remote sensing has a long history. It began in the 1970s from field spectral measurements in support of NASA's Landsat-1 data analysis. The term imaging spectrometer, rather than hyperspectral imager, was used more frequently from the perspective of instrumentation, especially at the beginning when it emerged as a new technology. The need for hyperspectral imaging came from the recognition based on laboratory and field spectral measurements, primarily of minerals and soils; multispectral imaging in four broad spectral bands with the Landsat's multispectral scanner (MSS) was not adequate to discriminate among, much less identify, minerals on the earth's surface that were important in resource exploration and environmental assessment.

In the 1970s, when geologists used Landsat MSS images to identify minerals, they found that many of the morphological clues of the minerals were absent in the four spectral band data and that the spectral reflectance was the major key to mapping geological units. Field measurements with portable spectrometers covering the wavelength range from 0.4 to 2.5 μm showed that spectral reflectance could be used to identify the mineralogy of exposed units, particularly if an OH-bond was present. Laboratory spectra of OH-bearing minerals clearly showed that spectrometers with a resolution of 10 nm FWHM or less were necessary to identify individual minerals. Landsat MSS had 100–200 nm wide bands, which are too wide to identify the individual minerals [30].

The need for hyperspectral imaging in vegetation analysis has spurred renewed interest in the potential for hyperspectral remote sensing. For example, the rates of ecosystem function reflected in the lignin to nitrogen ratio are important to understanding the land contribution to the carbon cycle. Moreover, hyperspectral imaging provides the only means of assessing the biochemistry of forest canopies remotely. Hyperspectral water color imaging is helpful in understanding the productivity and nutrient cycling in oceans for modeling the global carbon cycle. Phytoplankton distribution and variability is an important determinant of food-web structure aid trophodynamics, which ultimately control the flux of carbon in the oceans. Light in the visible region of the wavelength penetrates the ocean and lake water from a few centimeters to tens of meters, the depth depending on the amount of absorbing and suspended material in the water. The upwelling spectra can be decomposed into abundances of different phytoplankton groups: colored dissolved organic matter, detritus and suspended sediments. Hyperspectral imaging is a powerful tool in determining the composition of the suspended matter when all the above components are present. Remote sensing of snow and ice also needs hyperspectral imaging. For example, the extent of snow and ice cover changes dramatically with the season, and because of its high reflectance, it has a large effect on the earth's albedo. Snow reflectance depends on grain size, illumination angle, contaminants, and depth when the thickness is small. In the near-infrared region, ice is moderately absorbing and grain size has a large effect on the reflectance. In turn, the grain size is indicative of the thermodynamics of the snow and can give an indication of the beginning of melt.

The development of airborne hyperspectral imagers is a precursor of the hyperspectral satellites or spaceborne hyperspectral imagers. Firsthand experience acquired and lessons learned during the course of development airborne projects can significantly enhance the chance of success of the following space missions. Airborne instrument development helps elevate technical readiness level of spaceborne hyperspectral missions and significantly reduce their technical risks.

A. AIS, the First Airborne Hyperspectral Imager

The airborne imaging spectrometer (AIS) is the first hyperspectral imager for remote sensing. It was built in the early 1980s as an engineering test bed. At that time, neither the detectors,

Fig. 12. Exploded view of the AIS instrument (Courtesy of NASA/JPL).

optics, electronics, nor computers for rapid data analysis were readily available. In 1979, the first hybrid detector array became commercially available. This 2-D detector array consisted of a matrix of mercury cadmium telluride (or HgCdTe) detectors bonded to a matched silicon CCD readout array. AIS used the first hybrid infrared HgCdTe 2-D detector arrays, which contained only 32×32 pixels. Fig. 12 shows the exploded view of the AIS instrument. It is a pushbroom hyperspectral imager due to the use of a 2-D detector array as described in Section II-A. It covered a wavelength range in SWIR region from 1.2 to 2.4 μm with an SSI of 9.3 nm [28], [93].

AIS had several shortcomings. Among them, first it lacked a spectral coverage in the VNIR region. Second, it had a very narrow FOV of 3.7°, analogous to observing the earth from an aircraft through a soda straw. Third, because the detector array had 32×32 pixels, only a wavelength range of 32×9.6 nm $= 307$ nm could be covered. In order to expand the wavelength range from 1.2 to 2.4 μm, the grating of the AIS was designed to rotate through four positions within the 40 ms integration time it took the aircraft to move forward one cross-track line. Each rotation was 0.42° apart for moving the dispersed image across the detector array such that wavelength bands of 1.2−1.5 μm, 1.5−1.8 μm, 1.8−2.1 μm, and 2.1−2.4 μm are presented sequentially for readout. This technique was only partially successful, because of the time required for the grating to settle in a new position.

The AIS flew aboard the NASA C-130 aircraft over a number of geological targets in the western U.S., and over geobotanical targets and natural and agricultural vegetation across the U.S. It provided the first direct identification of minerals on the earth's surface from a remote imaging system. Hyperspectral data of ground scenes were acquired remotely first time onboard an aircraft. This allowed subtle spectral features to be observed that could not be seen in the multispectral data. The experiments of AIS flights and analyses of the acquired hyperspectral data provided valuable knowledge and useful experience for the development of hyperspectral imaging remote sensing. The best data were acquired when AIS was operating in the fixed grating position covering the 2.1–2.4 μm wavelength region, approximately the same range covered by the single Landsat Thematic Mapper Band.

The first successful hyperspectral data were obtained from a flight over the Cuprite Mining District, NV, USA in August 1983. After the individual band images were processed by normalizing each pixel to the scene average to bring out band-to-band

differences, spectral reflectance variations became apparent. It was historic that the first hyperspectral image acquired by AIS showed unambiguous evidence of mineral identification, in particular the minerals alunite and kaolinite. The spectral reflectance curves overlay those taken from laboratory spectra of samples taken from the same field locations.

A second AIS flight over the Cuprite Mining District was undertaken to double check the capability of the hyperspectral remote sensing. An unknown spectrum was fortuitous observed, which turned out to be the mineral buddingtonite, an ammonium feldspar after comparing with the known spectral libraries in the laboratory [31]. It was thought that buddingtonite might become a pathfinder mineral for gold. The success story of mineral identification, in particular the buddingtonite discovery, which became part of a public broadcasting system (PBS) documentary, led to a greater interest within NASA to pursue further technology development of hyperspectral imaging.

A later version of the instrument, AIS-2, incorporated a second-generation 64×64 pixels HgCdTe detector array, and covered the 0.8–2.4 μm spectral region. The promising hyperspectral imaging results, and the demonstrated need, led to the development of an imaging spectrometer program within NASA. In 1984, the initial program contained the next-generation aircraft system—the AVIRIS.

B. AVIRIS, the First Operational Airborne Hyperspectral Imager

Following the success of AIS, in 1983, A. F. H. Goetz and his colleagues at the JPL proposed to design and develop the AVIRIS. The goal was to introduce the newly available solid-state detector technology into remote sensing applications and to enable the acquisition of hyperspectral images in hundreds of contiguous spectral bands from VNIR to SWIR such that a complete radiance spectrum is available for each pixel [30].

The development of AVIRIS began in 1984. The AVIRIS was first flown aboard a NASA ER-2 aircraft at a 20 km altitude in 1986, the first science data delivered in 1987, and was fully operational since 1989. The AVIRIS is the best-known airborne hyperspectral imager in the community of terrestrial hyperspectral remote sensing. It is the first hyperspectral imager that measures the solar reflected spectrum from 400 to 2500 nm at 10 nm SSIs. It offers the best calibrated hyperspectral data resulting from its very high SNR and carefully designed calibration system and well implemented calibration procedure. As an operational airborne imaging spectrometer, AVIRIS is the primary provider of hyperspectral data to the research community since 1987. JPL has organized over ten workshops on AVIRIS since 1988. Numerous scientific papers related to AVIRIS have been published [41].

The AVIRIS is a whiskbroom hyperspectral imager using 1-D linear detector arrays. It covers a wavelength range of 0.4–2.45 μm with 224 spectral bands. It has a swath width of approximately 12 km containing 614 ground sampling cells of 20 m footprint from a 20 km altitude [41], [94]. AVIRIS is modular in construction, consisting of six optical subsystems and five electrical subsystems. In order to achieve the required spectral range, the AVIRIS design used four separate spectrometers (A
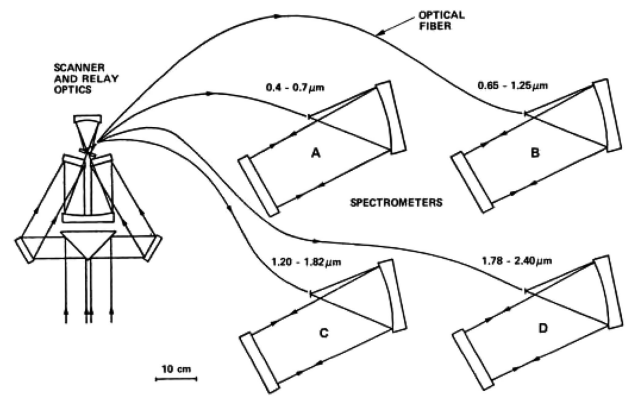

Fig. 13.   AVIRIS optics schematic (Courtesy of NASA/JPL).

to D), as shown in Fig. 13. Spectrometer A covers 0.4–0.7 μm; Spectrometer B covers 0.65–1.25 μm; Spectrometer C covers 1.20–1.82 μm; and Spectrometer D covers 1.78–2.40 μm. An all-reflective decentered aperture Schmidt design was selected for the spectrometers. All four spectrometers have the same basic optical layout and only the grating tilt changes significantly from Spectrometers A to D, as required by the spectral range covered by each of them. A silicon 32-element 1-D line detector array was selected for Spectrometer A, whereas three indium antimonide 64-element 1-D line detector arrays were used for Spectrometers B, C, and D. All the four detector arrays had a pitch size of 200 μm $\times$ 200 μm.

The design of AVIRIS has the following four key features.
1) Whiskbroom-scan architecture.
2) Four separate spectrometers, each covering a portion of the entire spectral range.
3) Very fast optics (F# 1).
4) Large detector pitch size (200 μm).

An advantage of the whiskbroom scan permits the use of 1-D linear detector arrays instead of 2-D area detector arrays. This yields easier and more accurate calibration while minimizing the number of artifacts that bother the design using 2-D area array detectors. The penalty of the whiskbroom-scan design is its limited integration time for ground sampling cells, because the total integration time for a cross-track line on the ground is shared by the 614 ground sampling cells when the spectrometers scan each of cross-track lines before the aircraft moves in the along-track direction to image the next cross-track line, as shown in Fig. 2. Maximizing throughput of the spectrometers is necessary in order to counteract the limited integration time. The last three features of AVIRIS design were aimed at maximizing the signal by providing maximum optical throughput and transmittance including grating efficiency. The point-scan (i.e., one ground sampling cell per scan) design requires a large aperture, which in the case of AVIRIS is 200 mm in diameter. The whiskbroom-scan architecture dominated the design of AVIRIS and yielded a large volume of the instrument.

Unlike AIS whose overall spectral range was achieved by rotating the grating through four positions, the AVIRIS design used four separate spectrometers, each covering a portion of the entire spectral range. This design eliminated the moving mechanism of the grating. It also removed the need of additional time
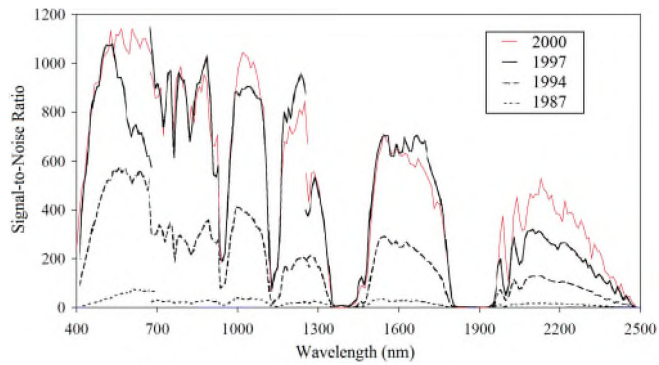
Fig. 14. Evolution of the improvement of SNR of AVIRIS instrument (Courtesy of NASA/JPL).

Fig. 15. Concept of CASI instrument and airplane operation in 1990s (Courtesy of ITRES Research).

used for settling the grating at each position and led to allocate more time for integration. Obviously, this design of using four separate spectrometers has a negative impact for reducing the volume and mass of the system. This design strategy is no longer being adopted given the fact that present available 2-D detector arrays have sufficient number of pixels in both dimensions for covering an entire range of wavelength and spanning a wide swath in the cross-track direction.

AVIRIS has undergone many modifications and upgrades over the years as technology advanced in detector arrays, electronics, and computing, which resulted in performance far exceeding original expectations. These upgrades have been reported in the literature [12]–[14], [24], [40], [79], [89]. Improvements to the focal planes cover five areas: multiplexer upgrades, signal chain noise reductions, photodiode array material optimization, blocking filter improvements, and an operating temperature change for the silicon detector array. These improvements significantly contribute to the increase of SNR of the AVIRIS [24]. Fig. 14 shows the curves of SNR of the AVIRIS instrument as a function of wavelength for the initial instrument in 1987 and after upgrading in years 1994, 1997, and 2000, respectively. It can be seen that the improvements are significant and encouraged. There are many useful experiences, know-how and lessons learned from the development of this high-end airborne instrument. These heritages of the airborne hyperspectral imager development have greatly benefited the development of spaceborne hyperspectral imagers.

C. Compact Airborne Spectrographic Imager (CASI), the First Commercial Airborne Hyperspectral Imager

In 1989, ITRES Research Limited based in Calgary, Canada marketed the CASI, a 2-D area CCD array based pushbroom hyperspectral imager [4], [98]. ITRES has been in commercial airborne hyperspectral imagers since then and extended their product line of hyperspectral imagers to cover SWIR and thermal regions of spectrum.

The design of CASI made use of the experience gained in constructing and operating the fluorescence line imager (FLI) instrument (see Section III-D). In 1988, ITRES built a proof-of-concept flyable hyperspectral imager prototype based on an earlier Space Shuttle instrument and deployed it on an airplane for summer flight campaigns. The results from the flights were
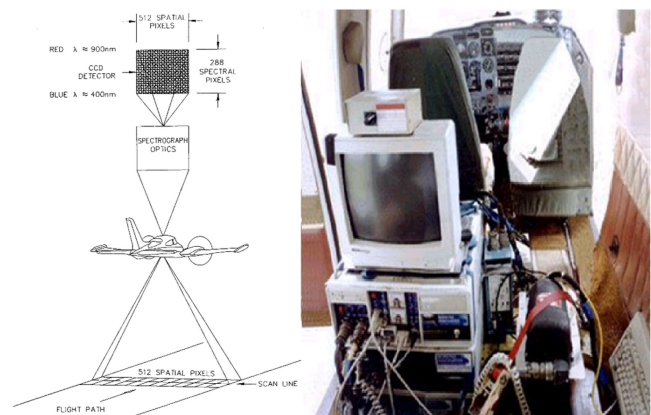
very encouraging in the areas of surface fish school surveys and spectral signature analysis [67], [87]. A commercial prototype was then built and operated in the summer of 1989 in a number of programs, including further capelin fish surveys, algae bloom and oil spill surveys and vegetation test site overflights. The first four production units of the CASI instrument were delivered to customers in Canada and Europe in the spring of 1990.

The initial version CASI employed an e2v 2-D area CCD array of size 612×576 pixels. It collects 288 spectral bands covering a spectral range from 400 to 926 nm with an SSI of 1.8 nm. It has a FOV of 35° corresponding to 578 pixels in the cross-track direction, typically reduced to 512 pixels for ease of data processing. This gives 1–5 km swath width on the ground depending on the altitude of the aircraft. The IFOV is 1.2 mill-radian (mrad), which corresponds to the ground sampling distance (GSD) of typically 2–5 m depending on altitude of the aircraft, ground speed, and integration time, as shown in Fig. 15 [3].

In the early 1990s, the data storage was the cartridge tape recorder that limited the rate of data recording. In order to achieve acceptable ground resolution during aircraft operation, data were normally collected in one of two modes: spatial mode or spectral mode. The spatial mode digitizes and records up to 15 spectral bands of information while maintaining full spatial resolution of 612 pixels of which the imaging field of view comprises 512 pixels. Each band is summed on-chip and may include any number of adjacent, nonoverlapping spectral rows. The spectral mode maintains full spectral elements 288 pixels encompassing the wavelength range specification of 400–926 nm. In this mode, up to 39 look directions, each of which corresponds to a single column on the CCD, can be defined for data acquisition. An individual single-row band at full spatial resolution, the scene recovery channel, is also recorded in order to create a high-resolution monochromatic reference image. Lately, a third mode (full-frame mode) had been added to the CASI instrument software. This mode digitizes and records the entire data frame of 612 by 288 pixels. The recording of this amount of data takes approximately 2 second per frame, making this mode useful mainly in laboratory situations for the acquisition of radiometric calibration data. It had also been used

in the field with a computer-controlled platform to synchronize the scanning motion of the platform with the acquisition of hyperspectral data frames.

In the early 2000s, ITRES upgraded the CASI by increasing its swath width and extending the spectral range. This upgraded version is referred to as the "CASI-1500," which is a 1500 spatial-pixel, 288 spectral-band hyperspectral imager with high throughput and sensitivity covering a spectral range of 365–1050 nm. It employs an ITRES' custom-designed CCD detector array specifically for use in hyperspectral applications. The CCD has a relatively large pitch size (20 μm $\times$ 20 μm) and provides relatively a large throughput and full-well capacity. Thanks to its outstanding performance, the CASI-1500 replaced the initial version CASI and became the main product of airborne hyperspectral imager of the company. Around 40 units have been sold worldwide.

The CASI-1500 is superbly adept for applications of low-albedo target hyperspectral imaging, such as water color remote sensing. More than one-third of all CASI-1500s sold are used for water applications. For example, the U.S. Naval Research Laboratory (NRL) owns a CASI-1500 spectrometer. NRL then used a slightly modified CASI-1500 spectrometer in their Hyperspectral Imager for Coastal Ocean (HICO) payload that was deployed in the International Space Station (ISS) in 2009. The HICO payload successfully operated on the ISS from 2009 until its demise in late-2014. More than 10 000 images of ocean and coastal areas were collected by HICO and distributed to the scientific community [48].

During the same period of time, ITRES has developed a line of airborne hyperspectral imager products by extending the spectral range from VNIR to SWIR, mid-wave infrared (MWIR), and thermal infrared (TIR), as well as widening the swath to span more spatial pixels. In addition to the scientific-grade hyperspectral imagers, ITRES has also developed three microversion commercial-grade hyperspectral imagers for use in UAVs, desktop and industrial imaging. These small and portable systems complement their full-size, scientific grade, high-performance siblings [84].

D. Canadian Hyperspectral Imaging Technology Development in 1980s and 1990s

The development of hyperspectral imaging technology in Canada began in early 1980s. The FLI is the first Canadian airborne hyperspectral imager. It was designed and constructed for Canada's federal government Department of Fisheries and Oceans (DFO) in 1981 as the first stage in developing an advanced satellite hyperspectral imager for remote sensing of the earth's surface. Canadian researchers and engineers pioneered this field, together with their American colleagues at NASA's JPL while building the FLI. Starting in 1983, the FLI flew over a wide variety of land and sea targets to acquire hyperspectral imagery with higher spectral resolution and sensitivity than other comparable hyperspectral imagers at the time [37], [39].

The FLI was built by Canadian companies (Moniteq Ltd. of Toronto and ITRES Research Ltd. of Calgary) and funded jointly by the DFO and the Interdepartmental Committee on Space (the predecessor of the Canadian Space Agency), which was at the
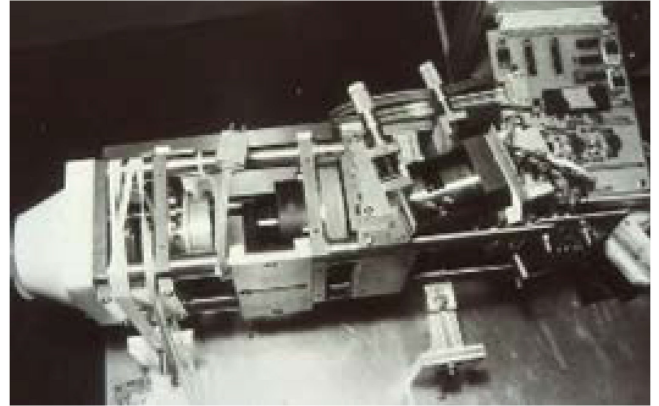

Fig. 16.   Photograph of the first Canadian airborne hyperspectral imager—FLI.

time responsible for Canada's space program. The eventual goal was to build a hyperspectral imager that could be launched as part of a satellite payload [37]. FLI used five 2-D area CCD detector arrays of format 385 $\times$ 288 pixels to cover a wide swath. Because the CCD frame rate was limited by the speed of the readout, the FLI operated in either spatial mode or spectral mode. In spatial mode, it operated in pushbroom mode with a FOV of 70° covered by 5 cameras for a total of 1925 pixels in a cross-track line, each pixel has an IFOV of 1.3 mrad, equivalent to 2.5 m GSD at altitude 2 km of the aircraft. In spectral mode, it operated in rake mode with 288 spectral bands covering a wavelength range from 430 to 800 nm. The optics consisted of a transmission grating with five lenses and effective f# 1.4. The key concept was the charge summation on chip to form bands, thus reducing data bandwidth and increasing SNR. The SNR of 1900:1 was achieved for a band of 16 elements. Fig. 16 shows the photograph of the FLI instrument.

The FLI flew a total of around 100 airplane campaigns in the period from 1984 to 1990 including the mapping of phytoplankton and benthic vegetation, and the measurement of water depths in lakes and coastal areas. The FLI had successfully mapped chlorophyll fluorescence, thereby fulfilling its design goal [38]. Observations also covered a wide variety of land targets and included projects in North America and Europe. In many of these cases, it was the same target molecule, the photosynthetic pigment chlorophyll a, whose fluorescence or absorption effects were being studied on land and in water.

As described in Section III-C, CASI had been fabricated commercially by ITRES Research Limited since 1989 [4]. In the early 1990s, about ten CASI instruments were in operation. These have increased the number of applications of hyperspectral remote sensing by providing a sensitive, flexible, and economical source of airborne hyperspectral imagery. The small volume of CASI had made it possible to fly on operational fish-counting surveys in light aircraft for fisheries management and on airborne water-depth mapping surveys with the hydrographic Lidar.

In addition to FLI and CASI that work in VNIR spectral region, the Canada Centre for Remote Sensing developed the first Canadian SWIR hyperspectral imager—SWIR Full Spectrographic Imager (SFSI) in 1992. The objective was to achieve
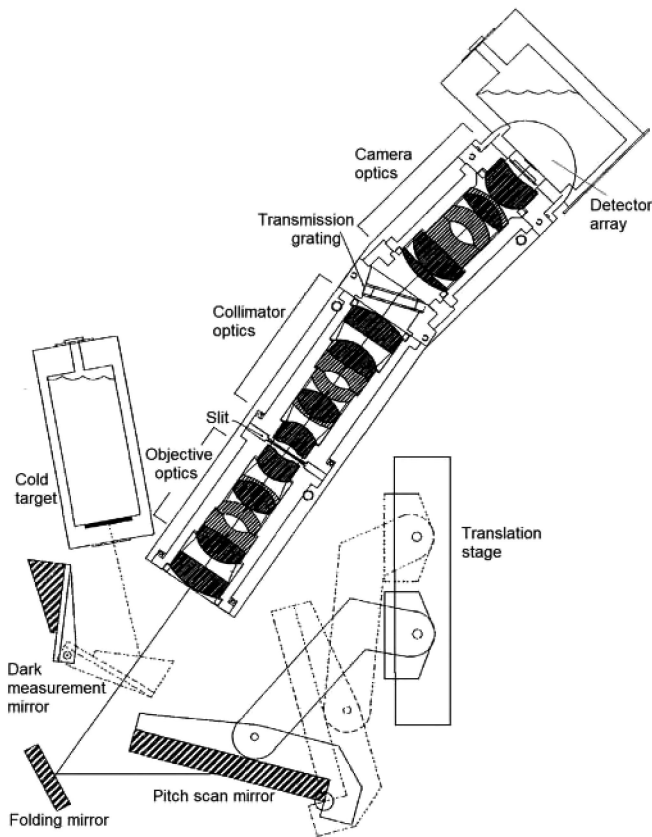
Fig. 17.   Optics and instrument assembly of the first Canadian airborne SWIR hyperspectral imager SFSI.

both high spectral resolution (10 nm) and high spatial resolution (0.5 m) from an airborne platform and to record the full spectrum for all image pixels. SFSI covers a spectral range from 1.2 to 2.4 μm in 122 contiguous spectral bands with 10 nm bandwidth. It utilizes a 2-D PtSi detector array, refractive optics, and a transmission grating. The fore-optics and spectrograph are f/1.8, and the FOV is 9.4°.

Fig. 17 shows the optics and instrument assembly of the SFSI instrument. SFSI provides a full image cube with an area coverage of 512 by 512 pixels [69].

Table I compares the specifications of the Canadian airborne hyperspectral imagers FLI, CASI, and SFSI with the AIS and AVIRIS in early years of hyperspectral technology development between 1980s and early 1990s. From the table, it can be seen that Canadian researchers and engineers pioneered the field hyperspectral instruments and applications. Canadian design and applications experience from the FLI and CASI were used to define the specifications for European Space Agency's (ESA's) Medium-Resolution Imaging Spectrometer (MERIS) on board ENVISAT satellite, which was launched in 2002.

During the period from the middle 1980s to late 1990s, several other airborne hyperspectral instruments were also being developed or were planned for the near future in other countries. Daedalus Inc. manufactured the multispectral infrared and visible imaging spectrometer (MIVIS) in 1993. It was a modular instrument with four hyperspectral spectrometers designed to collect radiation from the earth's surface in the visible,

near-IR, mid-IR, and thermal-IR regions with a total of 102 spectral bands. MIVIS was developed for use in environmental remote sensing studies across a broad spectrum of scientific disciplines [7].

An airborne hyperspectral imager called hyperspectral data and information collection experiment (HYDICE) was developed and flew in 1994 under the sponsorship of the U.S. NRL [86]. This instrument was designed around a prism dispersion concept and a single, hybrid HgCdTe 2-D array to cover a wavelength range of 0.4–2.5 μm. It had an IFOV of 0.5 mrad, equivalent to a 3 m footprint on the ground from a 6 km altitude. Although results were preliminary, SNR considerably exceeded those of the early version AVIRIS. Based on results from data analysis, HYDICE data could make possible the identification of materials that cover only 1-2% of a pixel, provided that their reflectance spectra are unique. The HYDICE began as a dual-use program; it soon reverted to an all Department of Defense (DoD) program.

Geophysical Environmental Research of Millbrook, NY developed the digital airborne imaging spectrometer (DAIS), which started operation in 1994. DAIS is an airborne hyperspectral imager with 79 spectral bands covering the visible and SWIR regions as well as the TIR [85].

Other commercial hyperspectral imagers in wavelength range from 0.4 to 2.5 μm were also developed. The one most like AVIRIS is the Australian Hyperspectral Mapper (HyMap) built by the HyVista Corporation. The design of HyMap was modular and this led to an ability to configure the spectral and spatial characteristics to suit the customer's specific requirements. The visible module includes a 2-D CCD detector array operated at ambient temperature, and the near infrared and short-wave infrared-1 (SWIR1) and 2 (SWIR2) modules incorporate InSb detector arrays cooled by liquid nitrogen to 77K. Each spectrographic module provides 32 spectral bands. Its FOV is 60° spanning 512 spatial pixels corresponding to a swath of 2.3 km with 5 m GSD at 1.3 km altitude or 4.6 km with 10 m GSD at 2.6 km altitude [15].

E. Planned NASA Spaceborne Hyperspectral Imagers in 1990s

The development of spaceborne hyperspectral imagers began in early 1980s. In late 1970s, JPL developed the shuttle multispectral infrared radiometer (SMIRR), which was scheduled to fly on the second flight of Space Shuttle (STS-2) in 1979 but was delayed until November 1981. The development of SMIRR could be considered as the beginning of the development of spaceborne hyperspectral imagers. SMIRR was installed in the payload bay of STS-2 alongside the shuttle imaging radar A. The purpose of the experiment was to test the feasibility of direct mineral identification using hyperspectral imaging from earth orbit. The instrument was designed as a profiler to acquire radiance data in ten spectral bands covering the VNIR and SWIR regions along a 100 m wide track beneath the spacecraft. The instrument consisted of a spare Mariner Venus-Mercury mission telescope with a rotating filter wheel in front of an HgCdTe detector array in the focal plane. Two 16 mm fighter-aircraft gun cameras recorded the ground track. The experiment was

TABLE I
SPECIFICATIONS OF THE CANADIAN AIRBORNE HYPERSPECTRAL IMAGERS IN OPERATION BETWEEN 1980S AND EARLY 1990S VERSUS THE AIS AND AVIRIS

| Parameters	FLI	CASI	SFSI	AIS	AVIRIS
Period of Operation	1984-1990	Since 1989	Since 1992	1983-1985	Since 1987
Country	Canada	Canada	Canada	USA	USA
Operation mode	pushbroom	pushbroom	pushbroom	pushbroom	whiskbroom
Detector array format	385×288	612×288	512×488	32×32	1×32 (A) 1×64 (C–D)
# of detector arrays (i.e. spectrometers)	5	1	1	1	4
Spectral range (nm)	430 – 805	418 – 926	1200 – 2400	1200–1500 (p1) 1500–1800 (p2) 1800–2100 (p3) 2100–2400 (p4)	410 – 700 (A) 680 – 1270 (B) 1250 – 1860 (C) 1840 – 2450 (D)
# of spectral elements	288	288	122	32 (32×4=128 after rotating the grating 4 positions)	224
Spectral sampling interval (nm)	1.3	1.8	10	9.3	10
# of spatial pixels	1925	512	512	32	614
Field-of-view (°)	70	35	11.7	3.7	30
IFOV (mrad)	1.3	1.2	0.4	1.9	1.0
Airplane altitude (km)	2	2	2	6	20
Swath width (km)	4.8	1 – 5	0.26	0.37	11
Spatial resolution (m)	2.5	2 – 5	0.5	11.4	20
Digitization	12	12	12	8	10
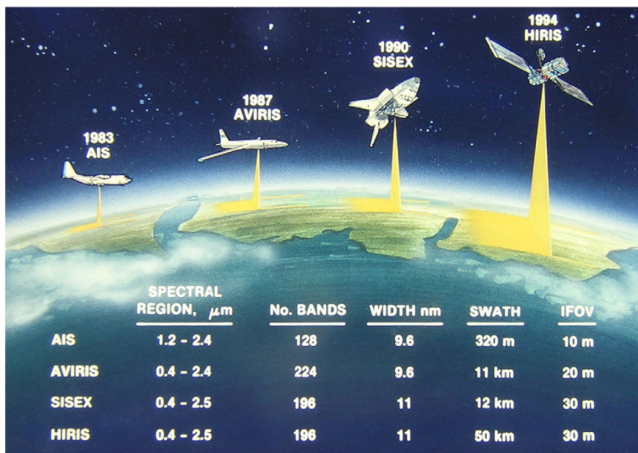
Fig. 18. NASA's plan of early time hyperspectral imaging program (Courtesy of NASA/JPL).

successful and resulted in the first direct identification of soil minerals from space through the use of the five spectral bands in the 2.2–2.5 μm region [29]. The minerals kaolinite and calcite, in the form of limestone were identified in an Egyptian dry lake and the surrounding hills and confirmed based on returned samples.

The promising results coming from AIS and SMIRR and the demonstrated needs led to the development of a hyperspectral imaging program within NASA. In 1984, the initial program contained the next-generation aircraft hyperspectral imager AVIRIS, the shuttle imaging spectrometer experiment (SISEX), and the free-flyer High-Resolution Imaging Spectrometer (HIRIS), as shown in Fig. 18. As described in Section III-B, AVIRIS successfully reached operational status, whereas SISEX was canceled after the space shuttle challenger disaster in 1986.

The HIRIS concept was developed further in 1988 in response to the earth observing system (EOS) flight proposal opportunity [22]. Its goal was to deploy on the EOS platform a hyperspectral imager covering the wavelength range 0.4–2.5 μm with 10 nm bandwidth for 196 contiguous spectral bands and spanning a 50 km swath from the 705 km orbital altitude [32]. The designed GSD (i.e., IFOV) was 30 m × 30 m. The HIRIS proposal was accepted for EOS, however, HIRIS did not fly as a result of the overall program was scaled back to approximately one-fourth of its original size.

At that time the earth observation community had not been sufficiently exposed to the advantages of hyperspectral imaging and they had not yet been able to work with high-quality hyperspectral datasets in order for them to become more familiar with the hyperspectral satellites. In addition, what scientific questions could be addressed uniquely with imaging spectrometry and, therefore, the community was not in a position to become a strong advocate for the hyperspectral satellite. At the time of the demise of HIRIS, only a handful of investigators had actually worked with hyperspectral data mainly because there existed only a few hyperspectral datasets, and they were of poor quality compared to what are available today. Additionally, there were not any readily available software tools to process the datasets that were orders of magnitude larger than the multispectral datasets from Landsat or SPOT satellites, and desktop and powerful computing systems were not yet up to the task. Therefore, it was not surprising that HIRIS was not included on EOS.

In the beginning of 1990s, NASA also worked with TRW to develop a spaceborne imaging spectrometry system called HyperSpectral Imager (HSI) for the LEWIS mission as a technology demonstration as part of its Small Spacecraft Technology Initiative (SSTI) program [21]. HSI was designed to have 128 bands in VNIR region of 0.4–1.0 μm and another 256 bands

in SWIR region of 0.9–2.5 μm, for a total of 384 bands. The SSIs in both spectral regions were 5.0 and 6.5 nm, respectively, which are still very competitive to the present-day spaceborne hyperspectral imagers. The swath width was 7.7 km and GSD was 30 m. Unfortunately, HSI was unsuccessful after its launch. Three days after the launch on August 23, 1997, the control of the satellite was lost and subsequently entered the earth atmosphere in September 1997 [56].

In November 2000, NASA launched Hyperion, a spaceborne hyperspectral imager built by TRW, aboard the Earth Observing-1 (EO-1) satellite [92]. If one compares the successful Hyperion with HIRIS, it can be easily seen that Hyperion carried some of the HIRIS instrument characteristics. EO-1 was created to develop and validate a number of instrument and spacecraft bus breakthrough technologies. It was intended to enable the development of future earth imaging observatories that would have a significant increase in performance while also having reduced cost and mass. EO-1 satellite is decommissioned in March 2017 after over 16 years of successful operation.

F. Hyperion, the First Spaceborne Hyperspectral Imager

Hyperspectral imager Hyperion onboard EO-1 satellite is well-known and often regarded as the first spaceborne hyperspectral imager in the remote sensing community. It was designed as a technology demonstration and provided calibrated spaceborne hyperspectral data for evaluation of hyperspectral applications [75]. Hyperion had a fast-track schedule of the development and was delivered to NASA Goddard Space Flight Center for spacecraft integration in less than 12 months. To achieve this goal, the developer TRW used focal planes and associated electronics remaining from the HSI for LEWIS mission under NASA SSTI program.

Hyperion is a pushbroom hyperspectral imager using 2-D area detector arrays. It had a relative narrow swath of 7.65 km. The ground footprint size is 30 m $\times$ 30 m. The 30 m size in the along-track direction was obtained by basing the frame rate on the velocity of the spacecraft for a 705-km orbit. The entire 7.65 km wide swath is obtained in a single frame. Each image is a data cube for 7.65 km wide in cross-track direction by 185 km long in along-track direction with 242 spectral bands [76]. The Hyperion instrument consisted of three physical units as shown in Fig. 19.

1) The Hyperion sensor assembly (HSA).
2) The Hyperion electronics assembly.
3) The cryocooler electronics assembly.

The HSA included a single telescope and two spectrometers: a VNIR spectrometer and a SWIR spectrometer. The telescope is a three-mirror anastigmat design with a 12-cm primary aperture and an effective F# of 11. Both VNIR and SWIR spectrometers are of three-reflector Offner form design using convex gratings. The telescope images the scene on ground onto a slit that defines an IFOV of 0.6240° by 0.0024°, which corresponds to a ground cross-track line of 7.65 km long (swath width) with 30 m wide in the satellite flight direction from an orbit of 705 km altitude. This slit image of the ground scene is relayed at a magnification of 1.38:1 to two focal planes of the VNIR and SWIR spectrometers. A dichroic filter (i.e., beam-splitter) in the
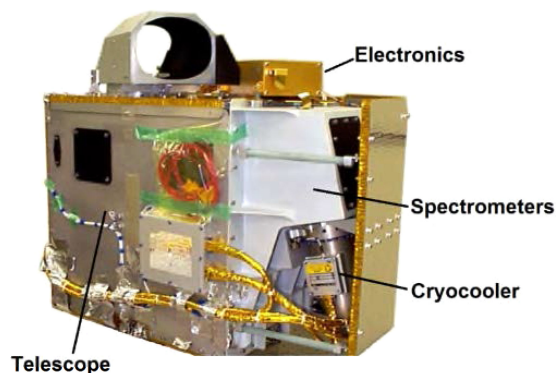

Fig. 19. Hyperion hyperspectral imager assembly (Source of NASA).

system reflects the spectrum from 400–1000 nm to the VNIR spectrometer and transmits the spectral from 900–2500 nm to the SWIR spectrometer. The SWIR overlap with the VNIR from 900 to 1000 nm allows cross-calibration of the two spectrometers. There is an order-sorting filter in the VNIR spectrometer.

The VNIR spectrometer used a 2-D CCD detector array of size 128 $\times$ 256 pixels, only a section of 70 (spectral) $\times$ 256 (spatial) pixels was used. The SWIR spectrometer used an HgCdTe detector array, and has 256 $\times$ 256 pixels of 60 μm pitch and a custom pixel readout. Only a 172 pixel (spectral) $\times$ 256 pixel (spatial) section was used. The two spectrometers produced a total number of 242 spectral bands.

The SNR of Hyperion was both modeled and measured under an assumption of 30% uniform albedo, a 60° solar zenith angle, a 10 nm spectral bandwidth, and a 224-Hz frame rate. The measured SNR is between 140:1 and 190:1 in VNIR region from 550 to 700 nm, 96:1 at 1225 nm, and 38:1 at 2125 nm. These measured SNR values are relatively low compared to those of the more recent spaceborne hyperspectral imagers, such as the Italian hyperspectral satellite PRecursore IperSpettrale della Missione Applicativa (PRISMA) [63] and the Advanced Hyperspectral Imager (AHSI) on GaoFen-5 (GF-5) satellite [57]. It is understandable that Hyperion was built in a short period of time as a technology demonstrator before this millennium. At that time, the technologies for detector arrays and their associated electronics as well as optics and the manufacture tools were less advanced than those in the recent years.

IV. SPACEBORNE HYPERSPECTRAL IMAGERS TO DATE AND UPCOMING

A. Summary of the Spaceborne Hyperspectral Imagers

The author of this article conducted a survey on spaceborne hyperspectral imagers to date and identified that there exist at least 25 hyperspectral imagers that have been deployed into orbits of earth, Moon, Mars, Venus, and comet for surface hyperspectral imaging remote sensing. Table II tabulates a list of hyperspectral imagers deployed in space in the order of launch years chronologically since the launch of the first spaceborne hyperspectral imager in late 1990s. This list may miss some spaceborne hyperspectral imagers. It is worth to note that during a short period from 2016 to 2019, nine spaceborne hyperspectral imagers have been launched into space. There is a leap for the

TABLE II
LIST OF SPACEBORNE HYPERSPECTRAL IMAGERS TO DATE AND UPCOMING

#	Hyperspectral Imager	Satellites / Platform	Orbit	Hyperspectral Imaging Approach	Launch Year	Demission Year	Spectral Range (μm)	Number of Spectral Bands	Spectral Sampling Interval (nm)	Ground Sampling Distance (m)	Swath Width (km)
1	SPIMs 1-5	MSX	LEO	Dispersive element	1996	2008	0.11−0.9	272	0.5−4.3	770	15
2	HSI	LEWIS	LEO	Dispersive element	1997	1997	0.4−1.0 0.9-2.5	128 256	5.0 6.5	30	7.7
3	Hyperion	EO-1	LEO	Dispersive element	2000	2017	0.4−2.5	220	10	30	7.7
4	CHRIS	PROBA	LEO	Dispersive element	2001	Active	0.4−1.0	19-62	1.25−11	25−50	13
5	MERIS	ENVISAT	LEO	Dispersive element	2002	2012	0.39−1.04	520 (transmit 15)	1.25	300	1150
6	VIRTIS	Rosetta	Comet 67P	Dispersive element	2004	2016	0.28−1.10 1.05−5.13	432 432	1.89 9.47	0.014°× 0.014° (IFOV)	3.67°× 3.67° (FOV)
7	VIRTIS	Venus Express	Venus	Dispersive element	2005	2015	0.28−1.10 1.05−5.13	432 432	1.89 9.47	0.014°× 0.014° (IFOV)	3.67°× 3.67° (FOV)
8	CRISM	MRO	Mars orbit (300 km)	Dispersive element	2005	Active	0.37−3.92	455	6.55	18	10.8
9	VIRTIS	NASA-Dawn	Vesta, Ceres	Dispersive element	2007	2018	0.28−1.10 1.05−5.13	432 432	1.89 9.47	0.014°× 0.014° (IFOV)	3.67°× 3.67° (FOV)
10	M3	Chandrayaan-1	Lunar orbit	Dispersive element	2008	2009	0.43−3.0	260	10	70	40
11	FTHSI	HJ-1A	LEO	Fourier Transform	2008	Active	0.45−0.95	115	4	100	50
12	HySI	IMS-1	LEO	Spectral filter	2008	2012	0.40−0.95	64	8	500	130
13	ARTEMIS	TacSat-3	LEO	Dispersive element	2009	2012	0.40−2.50	400	5	4	4
14	HICO	ISS	ISS orbit	Dispersive element	2009	2014	0.35−1.08	128	5.7	90	51
15	VNIS	Change'E	Lunar rover	Spectral filter	2013	2015	0.45-0.95 0.9-2.4	100	5	-	8.5°×8.5° (FOV)
16	OLCI	Sentinel-3A	LEO	Dispersive element	2016	Active	0.39−1.04	520 (transmit 21)	1.25	300	1270
17	MHRIS	GHGSat-D	LEO	Spectral filter	2016	Active	1.6−1.7	512	0.2	50	15
18	AaSI	Aalto-1	LEO	Spectral filter	2017	Active	0.50−0.90	6−20	7−10	192	97
19	DESIS	ISS	ISS orbit	Dispersive element	2018	Active	0.40−1.0	235	2.55	30	30
20	HyperScout	GomX-4B	LEO	Spectral filter	2018	Active	0.4−1.0	45	15	50	200
21	AHSI	GaoFen-5	LEO	Dispersive element	2018	Active	0.40−2.50	330	5 (VNIR) 10 (SWIR)	30	60
22	HysIS	IMS-2	LEO	Dispersive element	2018	Active	0.40−2.4	256	10	30	30
23	PRISMA	PRISMA	LEO	Dispersive element	2019	Active	0.40−2.51	237	12	30	30
24	HISUI	ISS	LEO	Dispersive element	2019	Active	0.40−2.50	185	10 (VNIR) 12.5 (SWIR)	30	20
25	HSI/ GISAT-1	GISAT	GEO	Dispersive element	July 2021 (scheduled)	N/A	0.38−1.0 0.9−2.5	158 256	3.92 (VNIR) 6.25 (SWIR)	318 191	160 190
26	EnMAP	German HS	LEO	Dispersive element	2021 (planned)	N/A	0.42−2.50	244	5 (VIRN) 10 (SWIR)	30	30
27	MAJIS	JUICE	Ganymede orbit (500 km)	Dispersive element	2022 (planned)	N/A	0.50−2.35 2.55−5.54	508 508	3.6 6.4	75	30
28	OCI	PACE	LEO	Dispersive element	2022 (planned)	N/A	0.34−0.89 0.94−22.6	110 7	5 (UVNIR) ? (SWIR)	1000	2663
29	HyspIRI	HyspIRI	LEO	Dispersive element	No launch date	N/A	0.38−2.5 3.9−12.0	212 8	10 (VSWIR) 80−540 (TIR)	60	150
30	FLORIS	FLEX	LEO	Dispersive element	2024 (planned)	N/A	0.50−0.74 0.68−0.78	132 288	1−2 (LR) 0.1−0.5 (HR)	300	150
31	CHIME	CHIME	LEO	Dispersive element	2029 (planned)	N/A	0.4−2.5	210	10	20−30	120

Active to when the manuscript was written on June 3, 2021.

number of spaceborne hyperspectral imagers launched in 2018. Several new spaceborne hyperspectral imagers have been under development for years or have been planned and will come up.

In terms of the platforms and orbits of these spaceborne hyperspectral imagers, majority of them (19 of them) are aboard satellites on low earth orbits (LEOs), including three of them deployed on the ISS. Six hyperspectral imagers are out of earth orbits, one (CRISM) on a Mars orbit, one (M3) on a lunar orbit, and one (VNIS) on a lunar rover for *in situ* observation. The Visible and Infrared Thermal Imaging Spectrometer (VIRTIS) and its two slight variants were deployed onboard the space probes of three planetary missions on orbits of a comet, Venus and two protoplanets.

With respect to the type of the instrument (or spectral dispersion means), 19 spaceborne hyperspectral imagers are dispersive elements based imaging spectrometers (discussed in Section II-A), using either gratings or prisms to disperse spectrum. Five hyperspectral imagers are spectral filter based imaging instruments using spectral filters to separate radiation light (discussed in Section II-B). Among these five, two of them use LVFs to disperse spectrum. These two imagers are HySI onboard the IMS-1, and HyperScout on ESA's GomX-4B nanosatellite. Three of them

utilize ETFs, of which VNIS uses AOTF, whereas Miniature High-Resolution Imaging Spectrometer (MHRIS) and AaSI use tunable Fabry–Pérot filters. There is only one spaceborne hyperspectral imager that uses Fourier transform interferometer to disperse spectrum (discussed in Section II-C). There is none spaceborne hyperspectral imager that uses snapshot hyperspectral imaging technology so far.

Regarding the operation mode, among the 25 spaceborne hyperspectral imagers listed in Table II, all of them use 2-D area detector arrays and operate in pushbroom mode. There is not a single spaceborne hyperspectral imager that uses 1-D linear detector arrays and operates in whiskbroom mode.

In Table II, six upcoming spaceborne hyperspectral imagers are also listed. They are: Environmental Mapping and Analysis Program (EnMAP), Moons and Jupiter Imaging Spectrometer (MAJIS), Ocean Color Instrument (OCI), Hyperspectral Infrared Imager (HyspIRI), Fluorescence Imaging Spectrometer (FLORIS), and Copernicus Hyperspectral Imaging Mission for the Environment (CHIME). EnMAP is a well-known high-performance hyperspectral imager for earth observation in remote sensing community, because it has been under development for over ten years and scientific user community is expecting it to come out.

Due to the large data volume generated by hyperspectral satellites, onboard data compression is sometimes adopted to reduce the data volume to ease the data transmission to ground. At least, five spaceborne hyperspectral imagers have used or will use an onboard data compression unit. These are the four hyperspectral imagers on orbits: VIRTIS, CRISM, M3, and HISUI, as well as the one to be launched EnMAP [84].

B. Brief Description of the Spaceborne Hyperspectral Imagers

It can be seen from Table II that the earliest spaceborne hyperspectral imager was the ultraviolet and visible imagers and spectrographic imagers (UVISI) onboard the midcourse space experiment (MSX) mission of the U.S. DoD, which was launched in 1996 [74]. It consisted of five spectrographic imagers (SPIMs) covering a wavelength range from UV to VNIR regions and four UV and visible multispectral imagers (MSI). It is not popular because of its large GSD (770 m) and the nature as a military satellite. UVISI provided hyperspectral and multispectral capabilities in wavelength range from 110 to 900 nm [10]. It records data in a total of 1360 spectral bands simultaneously, with a 770 m GSD at nadir and a swath about 15 km wide.

The second earliest spaceborne hyperspectral imager was HSI for the LEWIS mission launched in 1997 [21] as a technology demonstration under the NASA's SSTI program. Unfortunately, HSI did not reach the orbit. Three days after the launch on August 23, 1997, the control of the satellite was lost, and subsequently the satellite entered the earth atmosphere in September 1997 [56].

Hyperspectral imager Hyperion onboard NASA's EO-1 satellite launched on November 21, 2000 is well known and is often regarded as the first spaceborne hyperspectral imager in the remote sensing community due to the other two earlier spaceborne hyperspectral imagers being less known. Hyperion has been discussed in Section III-F.

The Compact High-Resolution Imaging Spectrometer (CHRIS) onboard ESA's Project for On-Board Autonomy (PROBA) satellite was launched on October 22, 2001. The primary objective of PROBA satellite was to test a number of innovations in spacecraft platform design, such as attitude control and recovery from errors, autonomous operation with minimal intervention from the ground [5]. The CHRIS covers the wavelength only in VNIR region at combined GSD of 17–20 m or 34–40 m with a multiangle viewing capability and programmable spectral bandwidth. It acquires up to 62 spectral bands at 5–15 nm SSI in a wavelength range of 415–1050 nm. It has five operating modes, each of which has varied nominal number of bands, wavelength range, spectral bandwidth and the nominal GSD, with GSD decreasing as spectral bandwidth increases. At perigee, CHRIS provides a GSD of 17 m, over typical image areas 13 km square. The longevity of PROBA satellite is quite impressive. It is still running after over 19 years orbiting (as of June 2021).

The MERIS onboard ESA's ENVISAT satellite was launched on March 1, 2002 and retired in 2012 after ten years of successful operation. MERIS was the first wide swath (1150 km) spaceborne hyperspectral imager consisting of five identical imaging spectrometers mounted in a fan-out configuration on the optical bench each covering one-fifth of the wide swath. It had high spectral and radiometric accuracy developed for observing the color of oceans, both in the open ocean and in coastal zones to study the oceanic biology and marine water quality of the global carbon cycle and the productivity of these regions and the atmosphere and land surface related processes. It acquired hyperspectral images in VNIR region and operated in a pushbroom mode. By design, MERIS could record 520 spectral bands in the wavelength range from 390 to 1040 nm with the native instrument SSI of 1.25 nm. However, the MERIS was restricted by its downlink capability and transmitted only 15 channels, where each channel was an average taken over eight to ten native spectral elements of the detector arrays. The GSD varies in the cross-track direction, between 260 m at nadir and 390 m at swath extremities [6].

The VIRTIS was originally built for ESA's Rosetta cometary mission [20], which was the third cornerstone mission of the ESA's Horizon 2000 program. Rosetta was a space probe, including an orbiter and a lander Philae, launched on March 2, 2004 for studying comet 67P/Churyumov–Gerasimenko. The spacecraft reached the comet on August 6, 2014. During its journey to the comet, the spacecraft flew by Mars and the asteroids 21 Lutetia and 2867 Šteins. VIRTIS is one of the scientific payloads of the Rosetta orbiter to detect and characterize the evolution of specific signatures—such as the typical spectral bands of minerals and molecules—arising from surface components and from materials dispersed in the coma. VIRTIS is a hyperspectral imager with three focal planes in two channels. The mapping channel, referred to as VIRTIS-M, has two 2-D focal planes covering the visible region from 0.28 to 1.1 μm and infrared region from 1.05 to 5.13 μm. The spectroscopic channel, referred to as VIRTIS-H, has a single aperture covering a wavelength

range from 1.84 to 4.99 μm with fine SSI. VIRTIS-M generates a total of 432 spectral band images of size 256×256 pixels in the wavelength range 0.28–4.99 μm with SSI of 1.89 and 9.49 nm in visible region and infrared region, respectively.

The two slight variants of VIRTIS were also built and selected as a key instrument for ESA's Venus Express mission and NASA-Dawn mission. This makes the VIRTIS a great success story of one payload design for three planetary missions. Venus Express mission was to study the Venusian atmosphere and clouds in detail, and to study the plasma environment and the surface characteristics of Venus from orbit. Venus Express was launched on November 9, 2005 and entered the target Venus orbit at apoapsis on May 7, 2006 [78].

VIRTIS on Dawn space probe launched on September 27, 2007 is for studying two of the three known protoplanets of the asteroid belt, Vesta and Ceres. The space probe entered orbit around Vesta on July 16, 2011, and completed a 14-month survey mission before leaving for Ceres in late 2012. It then entered orbit around Ceres on March 6, 2015 [88].

The CRISM is a VNIR and infrared hyperspectral imager onboard the NASA's spacecraft of Mars Reconnaissance Orbiter (MRO), which was launched on August 12, 2005 and attained Martian orbit on March 10, 2006. CRISM is one of the six major science instruments on MRO and still active after over 15 year operation on Martian orbit. It is used to produce detailed maps of the surface mineralogy of Mars and to identify minerals and chemicals indicative of the past or present existence of water on the surface of Mars [66]. CRISM acquires hyperspectral images from 362 to 3920 nm with an SSI of 6.55 nm. It operates in three modes: multispectral mode, targeted mode, and atmospheric mode. In the multispectral mode, it points at planet nadir to reconnoiter Mars with 72 of its 544 spectral bands at a footprint size of 100–200 m per pixel. Nearly the entire planet can be mapped in this fashion. The objective of this mode is to identify new scientifically interesting locations that could be further investigated. In targeted mode, it measures radiation reflected from Mars surface in all 544 spectral bands. When the MRO spacecraft is at an altitude of 300 km, it detects a scene of interest at full spatial resolution (15–19 m/pixel) and full spectral resolution (362–3920 nm at 6.55 nm/band). In atmospheric mode, it acquires only the emission phase function. Global grids of the resulting lower data volume observations are taken repeatedly throughout the Martian year to measure seasonal variations in atmospheric properties.

The Moon Mineralogy Mapper (M3) was a NASA contributed hyperspectral imager to India's first mission to the moon, Chandrayaan-1, launched on October 22, 2008. The M3 was the first high-resolution spaceborne hyperspectral imager operating in pushbroom mode to map the entire lunar surface spatially and spectrally. It generated images of moon surfaces in long narrow strips in a wavelength range from 400 to 3000 nm with an SSI of 10 nm. This forms 260 spectral images for a scene of the lunar surface. The swath width is 40 km on the moon's surface at a moment. In a cross-track line, there were 600 pixels of footprint size 70 m $\times$ 70 m on the moon surface. The circumference of the moon is 10 930 km. With overlap, it takes more than 274 image swaths to completely map the moon

[65]. The Chandrayaan-1 mission was cut short at ten months in August 2009, when contact was lost with the spacecraft. Despite the abbreviated mission, M3 was able to meet its mission requirements: collecting more than 95% of the Moon in global mode along with a small number of target mode images [8].

FTHSI onboard Chinese HJ-1A satellite is a Fourier transform imaging interferometer as discussed in Section III-C. Unlike dispersive element based hyperspectral imagers, a Fourier transform based hyperspectral imager produces interferometric data in Fourier transform domain, which need to be processed before obtaining radiometric data. The FTHSI instrument has a total of 115 bands covering a spectral range from 0.45 to 0.95 μm after processing of the raw Fourier transform data and returning to spectral domain. The width of the swath is 50 km with the ground footprint size 100 m [100]. The minisatellite constellation HJ is a China's national program for disaster monitoring and mitigation using remote sensing technology and for improvement of the efficiency of disaster mitigation and relief. The HJ-1 constellation includes three minisatellites referred to as HJ-1A, HJ-1B, and HJ-1C. HJ-1A and HJ-1B satellites were launched on September 6, 2008.

HySI onboard IMS-1 launched on April 28, 2008 was a 64-band VNIR imaging spectrometer with spatial sampling distance of about 500 m and swath width of about 130 km. It was aimed at validating the design of hyperspectral imager and providing hands on experience for users and scientists of the hyperspectral applications [53]. HySI was a spectral filter based hyperspectral imager. Unlike the traditional dispersive element (e.g., grating or prism) based instruments, HySI used an optical wedge filter, also known as an LVF, to disperse spectrum. It was the first spaceborne hyperspectral imager that used an LVF as the dispersive element. HySI consisted of only a telescope, a 2-D detector array with the wedge filter mounted very close to it and the associated front-end electronics. This is because an LVF-based hyperspectral imager omits a bulky spectrometer for dispersion of spectrum, thus it is much compact in volume and light in weight. The operational principle of an LVF-based hyperspectral imager is different from that of a dispersive element based hyperspectral imager, which has been discussed in Section II-B.

The Advanced Responsive Tactically Effective Military Imaging Spectrometer (ARTEMIS) was onboard TacSat-3 satellite launched on May 19, 2009. TacSat-3 was the third in a series of U.S. DoD military reconnaissance satellites. The TacSat satellites are designed to demonstrate the ability to provide real-time data collected from space to combatant commanders in the field [58]. The ARTEMIS hyperspectral imager used a single 2-D HgCdTe detector array covering both VNIR and SWIR spectral regions from 0.4 to 2.5 μm at a uniform SSI of 5 nm with 4 m GSD and a swath width of 4 km. The 2-D HgCdTe detector array was extended for its sensitivity in the blue wavelengths in order to cover the full spectral range. This allowed a simple instrument design that uses only a single spectrometer to cover both VNIR and SWIR spectral regions and significant reduction of instrument complexity and cost [91].

The Hyperspectral Imager for the Coastal Ocean (HICO) was deployed on the ISS on September 23, 2009. It was the first

spaceborne hyperspectral imager designed for coastal ocean research [60]. HICO was built by using non-space-hardened, COTS spectrometer to demonstrate improved coastal remote sensing products including bathymetry, bottom types, water optical properties, and on-shore vegetation maps. HICO was a pushbroom imaging spectrometer operating in VNIR region from 380 to 960 nm with an SSI of 5.7 nm. It had a swath width of 51 km when the ISS altitude was 420 km. Its GSD was 100 m, which was much smaller than that of other spaceborne ocean color imagers (300 m of MERIS and 1000 m of MODIS ocean color bands). Even with such small GSD comparing to other ocean color imagers, it still achieved reasonably high SNR: peak SNR 470:1 at 480 nm, SNR > 200:1 in spectral range 400–600 nm [48]. During its five years life, it collected approximately 10 000 hyperspectral scenes of the earth. The data have enabled ocean color scientists and managers to assess data quality and apply the imagery to a variety of scientific and societal problems.

The VNIS was one of the main scientific payloads of China's lunar rover Yutu (means Jade Rabbit in Chinese) of the Chang'E 3 mission, which reached lunar orbit on December 6, 2013 and soft landed on the moon on December 14, 2013. VNIS is the first *in situ* spectral imaging detection in both the VNIR and SWIR regions on the lunar surface. It was a spectral filter based hyperspectral imager and used AOTF to separate spectrum of the input radiation light. It consisted of a VNIR hyperspectral imager covering a wavelength range of 0.45–0.95 μm and a SWIR spectrometer covering a wavelength range of 0.9–2.4 μm. The VNIR hyperspectral imager had a FOV of 8.5° × 8.5° for 256 × 256 pixels in the scene with 100 spectral bands of 2—7 nm spectral resolution, whereas the SWIR spectrometer had an FOV of 3.6° × 3.6° for a single pixel in the scene with 300 spectral bands of 3–12 nm spectral resolution [97]. Mounted on the Yutu in the front, the VNIS measured the radiance diffusely reflected from the Moon's surface of the solar illumination with a 45° view angle and acquired spectral and geometric data for determining the lunar surface mineral composition and performing comprehensive analysis of the chemical composition. The high resolution and effective spectral imaging data obtained by VNIS has provided valuable hyperspectral data for lunar scientific applications [45].

The Ocean and Land Color Imager (OLCI) is a VNIR pushbroom hyperspectral imager. It is one of the seven instruments onboard ESA's Sentinel-3A satellite launched on February 16, 2016. OLCI is the successor of MERIS onboard ESA's ENVISAT, which was out of service since April 2012 after ten years of operation. OLCI was designed to provide global and regional measurements of ocean and land surface with high radiative accuracy based on the heritage design from MERIS. Same as MERIS, OLCI consists of five identical fan-out arranged Dyson spectrometers with five focal plane arrays to cover the wide swath of 1270 km at a GSD of 300 m. Its revisit time with global coverage has been improved to three days, instead of 15 days of MERIS. OLCI transmits to ground 21 spectral channels, compared to the 15 of MERIS. A lesson learned from MERIS is the negative impact of the direct solar reflection at sea surface to the sensor, which is referred to as sun-glint. To minimize the impact of sun-glint OLCI adopted an asymmetric swath

with respect to the satellite ground track to avoid sun-glint. A cross-track tilt of 12.6° of the overall FOV is used that results in a maximum observation zenith angle slightly above 55° [71].

The MHRIS is a secondary payload onboard the GHGSat-D launched on June 22, 2016. It is a spectral filter based hyperspectral imager by using an ETF. It covers a wavelength range 1600–1700 nm with over 300 spectral bands of 0.1 nm bandwidth and has a 15 km ground swath with a spatial resolution of under 50 m. The MHRIS instrument uses InGaAs SWIR detector array of 640 × 512 pixels, of which GHGSat-D masks the area outside the central 512 × 512 array. GHGSat is a commercial venture for the measurement of greenhouse gas and air quality gas emissions from industrial sites using satellite technology [36]. It is a nanosatellite based on a low-cost and high-performance nanosat bus NEMO-AM made by University of Toronto, Institute for Aerospace Studies/Space Flight Laboratory [99]. It has a launch mass of 15 kg and a volume of approximately 25U (20 cm × 30 cm × 42 cm) plus a mezzanine of size 7 cm × 18 cm × 42 cm on one side (-X).

AaSI is a spectral filter based hyperspectral imager by using a tunable FPI developed by VTT Technical Research Centre of Finland. It is the main payload of the Aalto-1 nanosatellite that was launched on June 23, 2017. The Aalto-1 is based on a 3U CubeSat with a volume of 34 cm × 10 cm × 10 cm and a mass of ∼ 4 kg built mainly by the students at Aalto University in Finland. Its design life is two years and average power production is 4.8 W. AaSI is able to record 2-D spatial images of selected spectral bands in a spectral range from 500 to 900 nm with a spectral resolution 10–30 nm by electronically tuning the FPI. Filter apertures of 7 or even 19 mm can be reached with the piezo-actuated FPI [81].

The DLR Earth Sensing Imaging Spectrometer (DESIS) is a pushbroom hyperspectral imager operating in VNIR region from 400 to 1000 nm with a minimum SSI of 2.55 nm. It has a ground swath width of 30 km with a GSD of 30 m. It is hosted on the multiuser system for earth sensing mounted on the ISS launched on June 29, 2018 as part of the SpaceX CRS-15 logistics flight to the ISS and installed to the exterior of the ISS on August 27, 2018 [77]. The main difference between DESIS and majority of spaceborne hyperspectral imagers is that DESIS is equipped with a pointing mirror in front of the entrance slit. It can point in forward direction and back direction up to ±15°. It can operate in either the static mode with 3° angle steps or the dynamic mode with up to 1.5° change in viewing direction per second. When operating in the static mode, it allows acquiring hyperspectral data to produce BRDF products or stereo images. When operating in the dynamic mode, it allows continuous observations of the same targets with ground motion compensation to further improve SNR of the acquired hyperspectral data.

HyperScout is a miniaturized hyperspectral imager of size 1U (10 cm × 10 cm × 10 cm) developed by Cosine Research in the Netherlands. It is onboard ESA's nanosatellite GomX-4B, which is one of a pair of two 6U nanosatellites (GomX-4A and GomX-4B). These two nanosatellites were launched at the same time as secondary payloads on February 2, 2018 on a Long March 2-D vehicle from Jiuquan Satellite Launch Center (JSLC), China. HyperScout is one of the five demonstration payloads onboard GomX-4B. It is a spectral filter based

hyperspectral imager covering a spectral range from 400 to 1000 nm with a spectral bandwidth of 15 nm. An LVF is used to separate the spectrum before the radiance reaching on a 2-D CMOS detector array. Thanks to the omission of the spectrometer, HyperScout instrument consists of only a telescope, an LVF, a focal plane array, an instrument control unit and onboard data handling unit, which fit in a volume of 1U. HyperScout has a swath width on ground of 200 km with a grand sampling distance of 70 m [16].

The AHSI is the main payload of the Chinese GF-5 satellite, which was launched on May 8, 2018 for scientific research on the earth's atmosphere and terrestrial observation. GF-5 satellite carries six payloads, a hyperspectral imager, and an MSI for terrestrial earth observation, along with four atmospheric observation instruments. The objectives of AHSI are to address many key science questions and operational needs using remote sensing technology. AHSI has 330 spectral bands covering a wavelength range from 0.4 to 2.5 μm. The SSI is 5 nm in VNIR (0.4–1.0 μm) region and 10 nm in SWIR (1.0–2.5 μm) region. The GSD of AHSI is 30 m, which is the same as that of Hyperion, whereas the swath width of AHSI is 60 km, which is about eight times wider than that of Hyperion. The SNR of AHSI is also remarkably higher than that of Hyperion. For example, the achieved peak SNR of AHSI is 654:1 versus 190:1 of Hyperion [57].

The PRISMA is an Italian hyperspectral satellite aiming to qualify the technology, contribute to develop applications, and provide products to institutional and scientific users for environmental observation and risk management. It was launched into a sun synchronous orbit on March 22, 2019 [59]. PRISMA instrument is the core of the PRISMA mission and consists of a hyperspectral imager and panchromatic (PAN) camera. The hyperspectral imager operates in pushbroom mode. It is composed of a VNIR spectrometer and a SWIR spectrometer to cover spectral bands ranging from 400 to 1010 nm and from 920 to 2505 nm. It provides hyperspectral images of the earth with 30 m GDS, 30 km swath width and spectral bands at an SSI of 12 nm. The PAN camera provides images at spatial resolution of 5 m within a wavelength range of 400–700 nm, spatially coregistered to the hyperspectral images, so as to allow images fusion to sharpen the spatial resolution of the hyperspectral images [63].

HISUI includes an HSI and an MSI. HISUI was deployed onboard the Japan Experiment Module in the ISS, which was launched to the ISS on December 6, 2019 [62]. The HSI and MSI were made in two separate boxes and operate either independently or simultaneously. The HSI is a pushbroom hyperspectral imager. It consists of a VNIR spectrometer and a SWIR spectrometer to cover a wavelength range from 0.40 to 2.5 μm with a total of 185 spectral bands (57 VNIR + 128 SWIR). The SSI is 10.0 nm in the VNIR region and 12.5 nm in the SWIR region. Due to the constraint of optical design and the availability of large form 2-D detector arrays, the swath of HSI is 20 km, which is one-third of that of the MSI (60 km). To fill the gap between the swaths of two imagers, the HSI is equipped with a pointing mechanism, which can tilt the HSI for ±5° in cross-track direction to match the swaths of the two imagers [61]. To deal with the constraint of data downlink capacity of the ISS,

the hyperspectral and multispectral data generated by HISUI are partially transmitted to ground stations (about 10 GB/day ≈ 30 000 km^2). The rest data (about 300 GB/day ≈ 900 000 km^2) are recorded in removable mass memory storages that are shipped back to earth by cargo ships three or four times a year.

Geo Imaging Satellite (GISAT) is an Indian imaging satellite class in geostationary orbit with a frequent revisit capability (i.e., high temporal resolution) for providing near real-time imaging and monitoring, which is scheduled to be launched in July 2021. There are two identical GISAT satellites. Each satellite carries an HSI and an MSI. The HSI consists of a VNIR spectrometer covering a wavelength range from 0.38 to 1.0 μm with a GSD of 318 m and a SWIR spectrometer covering a wavelength range from 0.9 to 2.5 μm with a GSD of 191 m. The MSI has six spectral bands covering a wavelength range from 0.45 to 0.875 μm with a GSD of 42 m. GISAT satellites acquire images in multispectral and hyperspectral bands to provide near real-time observation of large areas of India, under cloud-free conditions, for selected field image in every 5 min and entire Indian landmass image every 30 min at 42–318 m spatial resolution [90].

C. Upcoming Spaceborne Hyperspectral Imagers

There are at least six well-known spaceborne hyperspectral imagers that are under development or planned, some of them are upcoming soon.

The EnMAP is a German hyperspectral satellite mission scheduled to be launched in 2021. It aims at monitoring and characterizing the earth's environment on a global scale by providing high-quality hyperspectral data. EnMAP is a dispersive element (using prisms) based hyperspectral imager operating in pushbroom mode. It has 242 spectral bands covering a wavelength range from 420 to 2450 nm with an SSI of 6.5 nm for VNIR bands and 10 nm for SWIR bands. Its ground swath width is 30 km with a GSD of 30 m × 30 m. It is designed to achieve better SNR than the available spaceborne hyperspectral imagers. The SNR will be greater than 500:1 for a 10 nm equivalent bandwidth of the spectral band at 495 nm. In the SWIR region, an SNR of more than 150:1 will be reached [50].

The MAJIS has been selected as one of the scientific payloads by ESA for its Jupiter Icy Moons Explorer (JUICE) mission intended to explore Jupiter and three of its icy moons: Europa, Callisto, and Ganymede. It is scheduled to be launched in June 2022. The spacecraft of the JUICE mission is targeted to fly by Callisto, Ganymede and Europa, then a one-year orbital phase around Ganymede [54]. The MAJIS hyperspectral imager is a dual grating spectrometer design with the VNIR spectrometer covering a spectral range from 0.5 to 2.35 μm and the infrared spectrometer covering a spectral range from 2.25 to 5.54 μm. The spectral and spatial resolution of MAJIS takes advantage of the up-to-date developments of detector technology with two times of 508 spectral bands to achieve a wide wavelength range of 0.5–5.5 μm at SSI of 3.6 nm for VNIR and 6.4 nm for infrared over 400 spatial pixels in a cross-track line. The IFOV of 150 μrad of the instrument corresponds to a footprint size of 75 m on Ganymede from a 500 km circular orbit over Ganymede and to a footprint size of 150 km for observations of the atmosphere of Jupiter when flies by it [42].

The OCI is a hyperspectral imaging radiometer onboard NASA's Plankton, Aerosol, Cloud, Ocean Ecosystem (PACE) satellite, which is scheduled to be launched in 2022. OCI will be the most advanced ocean color hyperspectral imager in NASA's history. Observing chlorophyll from space has a long heritage—NASA's Coastal Zone Color Scanner (CZCS), the first ocean color satellite, was launched in 1978. CZCS was a multispectral radiometer, and only collected image at a few spectral bands. OCI will collect hyperspectral images in a wavelength range from 340 to 890 nm in the UV to NIR spectrum with bandwidth at 5 nm or finer (e.g. 2.5 nm). It also acquires seven discrete spectral band images from 940 to 2260 nm in the SWIR region. The OCI scans from east to west at a rotation rate of 5.77 Hz, acquiring earth view data at a 1000 m × 1000 m GSD at nadir and an angular range of ±56.5° for a ground swath width of 2663 km. The fore-optics design of the OCI follows that of SeaWiFS, with a rotating telescope, a half-angle mirror, and a transmissive depolarizer (rather than reflective one as with CZCS and SeaWiFS). Dichroics direct the light to the following three different focal planes.

1) A blue spectrograph (340–605 nm) with wavelength separation by a grating and a 2-D CCD array.
2) A red spectrograph (600–890 nm) using the same approach as in 1).
3) A SWIR detection assembly with wavelength separation using dichroics/bandpass filters and photodiodes.

Like SeaWiFS, OCI will perform a tilt maneuver every orbit at approximately the subsolar point to avoid sun glint reflected off the ocean, looking 20° north (fore) in the northern hemisphere and 20° south (aft) in the southern hemisphere [68].

The HyspIRI mission aims to study the world's ecosystems and to provide critical information on natural disasters such as volcanoes, wildfires, and drought. The mission was recommended in the 2007 National Research Council Decadal Survey requested by NASA, NOAA, and USGS. HyspIRI will identify the type of vegetation and its health. The mission will provide a benchmark on the state of the world's ecosystems against which future changes can be assessed. The mission will also assess the carbon and other gases released from wildfires. The data from HyspIRI will be used for a wide variety of studies primarily in the carbon cycle and ecosystem and earth surface and interior focus areas. The HyspIRI satellite will be launched into a LEO orbit (no launch date). It will carry two instruments: a hyperspectral imager operating from the visible to short wave infrared (VSWIR) covering a wavelength range of 380–2510 nm in 10 nm SSI. An MSI acquires eight broadband images from 3.9 to 12 μm in the MWIR and TIR. The VSWIR and TIR instruments both have a spatial resolution of 60 m at nadir. The VSWIR will have a revisit rate of 19 days and the TIR will have a revisit rate of five days. With the technology advancement, current space computer capabilities allow for onboard real-time data processing, compression, and cloud screening. HyspIRI will equip with an intelligent payload module (IPM), which enables direct broadcast of a subset of the hyperspectral data processed onboard and downlinked to the ground in near real-time.

FLORIS for ESA's Fluorescence Explorer (FLEX) mission is a pushbroom hyperspectral imager. The FLEX satellite is scheduled to be launched in 2024 and will fly in tandem with the Sentinel 3 satellite, making use of data synergy with visible reflectance data from the OLCI [70] and surface temperature data from the Sea and Land Surface Temperature Radiometers (SLSTR) [17], [18]. FLORIS consists of two imaging spectrometers with a very narrow SSI to measure the vegetation fluorescence in the spectral range between 500 and 780 nm. The first imaging spectrometer (referred to as high-resolution spectrometer) measures the fluorescence spectrum within two oxygen absorption bands (O2A and O2B) at SSI between 0.1 and 0.5 nm in wavelength range of 677–780 nm. The second imaging spectrometer (referred to as low-resolution spectrometer) derives additional atmospheric and vegetation parameters at SSI between 1 and 2 nm in wavelength range of 500–740 nm. It acquires the hyperspectral images at a spatial resolution of 300 m over a swath of 150 km [19]. Observing the plant functional status from space represents a major interest for farming, forest management, and assessment of the terrestrial carbon budget. The measurement of solar-induced chlorophyll fluorescence directly addresses the photosynthetic efficiency of the terrestrial vegetation layer and complements traditional reflectance measurements used to infer parameters like leaf area index or chlorophyll absorption. Fluorescence estimates provide an early and more direct approach for diagnosis of the functioning and health status of vegetation. In fact, the fluorescence emission is in competition with the photochemical conversion and may allow more accurate carbon assimilation estimation and earlier stress detection than is possible from only reflectance data.

The CHIME will provide routine hyperspectral observations to support new and enhanced services for sustainable agricultural and biodiversity management, and soil property characterization. It will complement Copernicus Sentinel-2 satellite for applications such as land-cover mapping. The CHIME mission is part of the expansion of the Copernicus Space Component programme of the ESA, in partnership with the European Commission. The satellite will acquire hyperspectral data with high radiometric accuracy in the VSWIR range (400–2500 nm) at 10 nm spectral resolution. The CHIME hyperspectral imager will have a spatial resolution of 20–30 m and 128 km swath width to achieve a revisit time of 10–12.5 days. The satellite will be launched into a sun synchronous LEO orbit with an overpass time of between 10:30 and 11:30 local time on descending node. The core products supplied by the mission will be Level-2A atmospheric and geometrically corrected surface reflectance, including bottom-of-atmosphere reflectance, ortho-rectified geometry using a digital elevation model, and pixel classification (a side product from the atmospheric correction process) allowing users to distinguish opaque clouds, thin clouds, cloud shadows, vegetation, etc. In addition, a set of downstream products will be proposed to users as part of the mission catalog to support the operational use of the data [72], [73].

V. CONCLUSION

Hyperspectral imaging is a powerful remote sensing technology, which records a full spectrum from VNIR to SWIR for each pixel of an image. The scientific rationale for hyperspectral imaging is evident given its strong needs from the diversity of

disciplines. Based on high spectral resolution measurements of radiation light interacting with matter, it allows the characterization and quantification of surface materials. Quantitative variables derived from the observed spectra, e.g., directly through distinct absorption features, are diagnostic information of the surface materials of earth or planets.

Thanks to well-established spectroscopic techniques, hyperspectral imaging remote sensing has the potential to deliver significant enhancement in quantitative value-added products reflecting the status of various terrestrial and aquatic ecosystems and the changes they undergo. This will support the generation of a wide variety of new products and services in the domain of agriculture, food security, raw materials, soils, biodiversity, environmental degradation and hazards, inland and coastal waters, and forestry. These are relevant to various policies that are currently not being met or can be really improved but also to the private downstream sector. Hyperspectral imaging remote sensing allows optimal mapping of targets with well-defined optical signatures, flexible band placement for minimizing and estimating the effects of atmospheric scattering and absorption, and accurate simulation of the responses of other sensors.

This article provides an overview of hyperspectral satellites and their development history. It begins with the introduction of hyperspectral satellites followed by the description of the principle of hyperspectral imaging implemented by the four types of instruments for spectral imaging: dispersive elements based instrument, spectral filters based instrument, Fourier transform based imaging interferometer, and snapshot hyperspectral imagers. The article reviews the history of the development of hyperspectral imaging technology by telling stories of the development from airborne instruments to spaceborne instruments, starting from the first airborne hyperspectral imager in the world—AIS built in early 1980s, followed by the first operational airborne hyperspectral imager—AVIRIS developed since middle 1980s, then the first commercial airborne hyperspectral imager—CASI fabricated since late 1980s. The description of the history of hyperspectral imaging continues with the development of hyperspectral technology in Canada between 1980s and 1990s, and the NASA planned orbiting hyperspectral imagers in 1990s, until the launch of the first spaceborne hyperspectral imager—Hyperion onboard EO-1 satellite in 2000.

The author of the article carried out a survey on spaceborne hyperspectral imagers to date. This article summarizes the survey. There exist at least 25 hyperspectral imagers that have been deployed into space. The summary was made in the order of launch years chronologically since the beginning of the development and in terms of the orbits of the satellites, the imaging approach of the hyperspectral imagers, and their operational mode. A total of 19 hyperspectral imagers have been deployed aboard satellites orbiting the earth, including three of them on the ISS. Six of them are out of earth orbits, including one on a Mars orbit, one on a lunar orbit, one on a lunar rover for *in situ* observation, one plus its two variants deployed onboard the space probes of three planetary missions on orbits of a comet, Venus and two protoplanets. Regarding the imaging approach, 19 hyperspectral imagers are dispersive element based instruments, using either gratings or prisms to separate spectrum. Five hyperspectral imagers use spectral filters

to separate spectrum. Only one spaceborne hyperspectral imager uses Fourier transform interferometer to disperse spectrum. All the 25 spaceborne hyperspectral imagers use 2-D area detector arrays and operate in pushbroom mode. The article briefly describes the 25 spaceborne hyperspectral imagers and their mission objectives with the focus on the instrument performance parameters and technical features.

At least six well-known spaceborne hyperspectral imagers are under development or planned and are upcoming soon. These are EnMAP, MAJIS, OCI, HyspIRI, FLORIS, and CHIME. This article also briefly describes them and reviews their mission objectives with the focus on the instrument performance parameters and technical features.

REFERENCES

[1] R. Abdlaty *et al.*, "Hyperspectral imaging: Comparison of acousto-optic and liquid crystal tunable filters," *Proc. SPIE*, vol. 10573, 2018, Art. no. 105732P.

[2] R. D. Alcock and J. M. A. Coupland, "Compact, high numerical aperture imaging Fourier transform spectrometer and its application," *Meas. Sci. Technol.*, vol. 17, no. 11, pp. 2861–2868, Nov. 2006.

[3] C. D. Anger, S. K. Babey, and R. J. Adamson, "New approach to imaging spectroscopy," *Proc. SPIE*, vol. 1298, 1990, pp. 72–86.

[4] S. K. Babey and C. D. Anger, "A compact airborne spectrographic imager (CASI)," in *Proc. IEEE 12th Can . Symp . Remote Sens . Geosci . Remote Sens . Symp .*, 1989, vol. 2, pp. 1028–1031.

[5] M. J. Barnsley, J. J. Settle, M. A. Cutter, D. R. Lobb, and F. Teston, "The PROBA/CHRIS mission: A low-cost smallsat for hyperspectral, multi-angle, observations of the earth surface and atmosphere," *IEEE Trans. Geosci. Remote Sens.*, vol. 42, no. 7, pp. 1512–1520, Jul. 2004.

[6] J.-L. Bézy, J.-P. M. Huot, S. M. Delwart, L. Bourg, R. Bessudo and Y. Delclaud, "Medium resolution imaging spectrometer for ocean colour onboard ENVISAT," in *Optical Payloads for Space Missions*, S.-E. Qian, Ed. Chichester, U.K.: Wiley, 2016, pp. 91–120.

[7] R. Bianchi *et al.*, "MIVIS airborne hyperspectral remote sensing in Europe," in *Proc. Int. Symp. Spectral Sens. Res.*, Melbourne, VIC, Australia, 1995.

[8] J. W. Boardman *et al.*, "Full-mission selenolocation progress for the Moon Mineralogy Mapper on Chandrayaan-1," in *Proc. 42nd Lunar Planet. Sci. Conf.*, 2011.

[9] R. Braun and R. Harig, "Identification and mapping of spilled liquids by passive hyperspectral imaging," *Proc. SPIE*, vol. 8546, 2012, Art. no. 85460F, doi: 10.1117/12.974496.

[10] J. F. Carbary, "Ultraviolet and visible imaging and spectrographic imaging instrument," *Appl. Opt.*, vol. 33, no. 19, pp. 4201–4213, 1994.

[11] C.-I. Chang, *Hyperspectral Data Processing*. Hoboken, NJ, USA: Wiley, 2013.

[12] M. L. Eastwood, C. M. Sarture, T. G. Chrien, R. O. Green, and W. M. Porter, "Current instrument status of the airborne visible/infrared imaging spectrometer (AVIRIS)," *Proc. SPIE*, vol. 1540, 1991, pp. 164–175.

[13] T. G. Chrien, "AVIRIS: Recent instrument maintenance, modifications and 1992 performance," in *Proc. Summaries 3rd Annu. JPL Airborne Geosci. Workshop*, Pasadena, CA, USA, 1992, pp. 78–97.

[14] T. G. Chrien, R. O. Green, C. M. Sarture, C. Chovit, M. L. Eastwood, and B. T. Eng, "Airborne visible/infrared imaging spectrometer (AVIRIS): Recent improvements to the sensor," in *Proc. Summaries 4th Annu. JPL Airborne Geosci. Workshop*, 1993, vol. 1, pp. 27–30.

[15] T. Cocks, R. Jenssen, A. Stewart, I. Wilson, and T. Shields, "The HyMap airborne hyperspectral sensor: The system, calibration and performance," in *Proc. 1st EARSeL Workshop Imag. Spectrosc.*, 1998, pp. 37–43.

[16] S. S. Conticello *et al.*, "Hyperspectral imaging for real time land and vegetation inspection," in *Proc. 4S Symp., Small Satell. Syst. Services*, 2016, pp. 1–15.

[17] P. Coppo *et al.*, "SLSTR: A high dual scan temperature radiometer for sea and land surface monitoring from space," *J. Mod. Opt.*, vol. 57, pp. 1815–1830, 2010.

[18] P. Coppo, C. Mastandrea, M. Stagi, L. Calamai, and J. Nieke, "Sea and land surface temperature radiometer detection assembly design and performance," *J. Appl. Remote Sens.*, vol. 8, 2014, Art. no. 084979.

[19] P. Coppo *et al.*, "Fluorescence imaging spectrometer (FLORIS) for ESA FLEX mission," *Remote Sens.*, vol. 9, 2017, Art. no. 649.

[20] A. Coradini *et al.*, "VIRTIS: An imaging spectrometer for the Rosetta mission," *Space Sci. Rev.*, vol. 128, no. 1–4, pp. 529–559, 2007.

[21] R. K. De Long, J. Marmo, D. P. Bowler, and T. E. Romesser, "Airborne and satellite imaging spectrometer development at TRW," *Proc. SPIE*, vol. 2480, 1995, pp. 287–294.

[22] J. Dozier, "HIRIS—The high resolution imaging spectrometer," *Proc. SPIE*, vol. 0924, 1988, pp. 23–30.

[23] J. D. Dwight *et al.*, "Compact snapshot image mapping spectrometer for unmanned aerial vehicle hyperspectral imaging," *J. Appl. Remote Sens.*, vol. 12, no. 4, 2018, Art. no. 044004.

[24] M. L. Eastwood *et al.*, "Recent improvements to the AVIRIS sensor: Flight season 2000," in *Proc. Airborne Visible/Infrared Imag. Spectrometer Workshop*, Pasadena, CA, USA, 2000, pp. 1–12.

[25] L. Gao, R. T. Kester, and T. S. Tkaczyk, "Compact image slicing spectrometer (ISS) for hyperspectral fluorescence microscopy," *Opt. Exp.*, vol. 17, no. 15, pp. 12293–12308, 2009.

[26] L. Gao *et al.*, "Depth-resolved image mapping spectrometer (IMS) with structured illumination," *Opt. Exp.*, vol. 19, no. 18, pp. 17439–17452, 2011.

[27] N. Gat, "Imaging spectroscopy using tunable filters: A review," *Proc. SPIE*, vol. 4056, pp. 50–64, 2000.

[28] A. F. H. Goetz, U. Vane, J. Solomon, and B. N. Rock, "Imaging spectrometry for earth remote sensing," *Science*, vol. 228, pp. 1147–1153, 1985.

[29] A. F. H. Goetz, L. C. Rowan, and M. J. Kingston, "Mineral identification from orbit: Initial results from the shuttle multispectral infrared radiometer," *Science*, vol. 218, pp. 1020–1024, 1982.

[30] A. F. H. Goetz, "Imaging spectrometry for remote sensing: Vision to reality in 15 years," *Proc. SPIE*, vol. 2480, pp. 1–13, 1995.

[31] A. F. H. Goetz and V. Srivastava, "Mineralogical mapping in the Cuprite Mining District, Nevada," in *Proc. Airborne Imag. Spectrometer Data Anal. Workshop*, 1985, vol. 85, pp. 22–31.

[32] A. F. H. Goetz and M. Herring, "The high resolution imaging spectrometer (HIRIS) for EOS," *IEEE Trans. Geosci. Remote Sens.*, vol. 27, no. 2, pp. 136–144, Mar. 1989.

[33] H. Grahn and P. Geladi, *Techniques and Applications of Hyperspectral Image Analysis*. Hoboken, NJ, USA: Wiley, 2007.

[34] B. Geelen, N. Tack, and A. Lambrechts, "New multi- and hyperspectral cameras cover diverse applications," *Photonics Spectra*. Accessed: Mar. 2013. [Online]. Available: https://www.photonics.com/Articles/New_Multi-_and_Hyperspectral_Cameras_Cover/a53223

[35] S. Germain *et al.*, "Global monitoring of greenhouse gas emission," in *Proc. 30th Annu. AIAA/USU SmallSat Conf.*, Logan, UT, USA, Aug. 2016 SSC16-III-11.pp1-7.

[36] S. Germain, GHGSat-D—Global emissions monitoring GHGSat, Inc., 2019. [Online]. Available: https://www.ghgsat.com/our-platforms/claire/

[37] J. F. R. Gower, G. A. Borstad, L. H. Gray, and H. R. Edel, "The fluorescence line imager: Imaging spectroscopy over water and land," in *Proc. 11th Can. Symp. Remote Sens.*, Waterloo, ON, Canada, Jun. 22–25, 1987, pp. 689–697.

[38] J. F. R. Gower and G. A. Borstad, "Mapping of phytoplankton by solar-stimulated fluorescence using an imaging spectrometer," *Int. J. Remote Sens.*, vol. 11, pp. 313–320, 1990.

[39] J. F. R. Gower, G. A. Borstad, C. D. Anger, and H. R. Edel, "CCD-based imaging spectroscopy for remote sensing: The FLI and CASI programs," *Can. J. Remote Sens.*, vol. 18, no. 4, pp. 199–208, 1992.

[40] R. O. Green *et al.*, "Airborne visible/infrared imaging spectrometer (AVIRIS): Recent improvements to the sensor and data facility," *Proc. SPIE*, vol. 1937, 1993, pp. 180–190.

[41] R. O. Green *et al.*, "Imaging spectroscopy and the airborne visible/infrared imaging spectrometer (AVIRIS)," *Remote Sens. Environ.*, vol. 65, no. 3, pp. 227–248, 1998.

[42] I. Guerri *et al.*, "The optical design of the MAJIS instrument on board of the JUICE mission," *Proc. SPIE*, vol. 10690, 2018, Art. no. 106901L.

[43] N. Hagen, R. T. Kester, L. Gao, and T. S. Tkaczyk, "Snapshot advantage: A review of the light collection improvement for parallel high-dimensional measurement systems," *Opt. Eng.*, vol. 51, 2012, Art. no. 111702.

[44] N. Hagen and M. W. Kudenov, "Review of snapshot spectral imaging technologies," *Opt. Eng.*, vol. 52, no. 9, Sep. 2013, Art. no. 090901.

[45] Z. P. He, R. Shu, and J. Y. Wang, "Imaging spectrometer based on AOTF and its prospects in deep-space exploration application," *Proc. SPIE*, vol. 8196, 2011, Art. no. 819625.

[46] R. Horstmeyer *et al.*, "Flexible multimodal camera using a light field architecture," in *Proc. IEEE Int. Conf. Comput. Photogr.*, 2009, pp. 1–8.

[47] IMEC, "Meadia release: IMEC demonstrates shortwave infrared (SWIR) range hyperspectral imaging camera," SPIE Photonics West , San Francisco, CA, USA, 2018.

[48] M. E. Kappus *et al.*, "Hyperspectral imager for the coastal ocean on the international space station," in *Optical Payloads for Space Missions*, S.-E. Qian, Ed. Chichester, U.K.: Wiley, 2016, pp. 29–49.

[49] M. Kastek *et al.*, "Method of gas detection applied to an infrared hyperspectral sensor," *Photon. Lett. Poland*, vol. 4, no. 4, pp. 146–148, 2012.

[50] H. Kaufmann *et al.*, "Environmental mapping and analysis program—A German hyperspectral mission," in *Optical Payloads for Space Missions*, S.-E. Qian, Ed. Chichester, U.K.: Wiley, 2016, pp. 161–181.

[51] M. W. Kudenov and E. L. Dereniak, "Compact snapshot birefringent imaging Fourier transform spectrometer," *Proc. SPIE*, vol. 7812, 2010, Art. no. 781206.

[52] M. W. Kudenov and E. L. Dereniak, "Compact real-time birefringent imaging spectrometer," *Opt. Exp.*, vol. 20, no. 16, pp. 17973–17986, 2012.

[53] A. S. K. Kumar and D. R. M. Samudraiah, "Hyperspectral imager onboard Indian Mini Satellite-1," in *Optical Payloads for Space Missions*, S.-E. Qian, Ed. Chichester, U.K.: Wiley, 2016, pp. 141–160.

[54] Y. Langevin *et al.*, "The MAJIS VIS-NIR imaging spectrometer for the JUICE mission," in *Proc. 45th Lunar Planet. Sci. Conf.*, The Woodlands, TX, USA, 2014, p. 2493.

[55] M. Levoy *et al.*, "Light field microscopy," *ACM Trans. Graph.*, vol. 25, no. 3, pp. 924–934, 2006.

[56] Lewis (SSTI 1), 2014. Accessed: June 29, 2021. [Online]. Available: http://space.skyrocket.de/doc_sdat/lewis.htm

[57] Y.-N. Liu *et al.*, "The advanced hyperspectral imager aboard China's GaoFen-5 satellite," *IEEE Geosci. Remote Sens. Mag.*, vol. 7, no. 4, pp. 23–32, Dec. 2019.

[58] R. B. Lockwood *et al.*, "Advanced responsive tactically-effective military imaging spectrometer (ARTEMIS) design," in *Proc. IEEE Int. Symp. Geosci. Remote Sens.*, 2006, pp. 1628–1630.

[59] R. Loizzo *et al.*, "PRISMA: The Italian hyperspectral mission," in *Proc. IEEE Int. Geosci. Remote Sens. Symp.*, 2018, pp. 175–178.

[60] R. L. Lucke *et al.*, "Hyperspectral imager for the coastal ocean: Instrument description and first images," *Appl. Opt.*, vol. 50, pp. 1501–1516, 2011.

[61] T. Matsunaga *et al.*, "Hyperspectral imager suite (HISUI): Japanese spaceborne hyperspectral imager for resource and environmental mapping," in *Optical Payloads for Space Missions*, S.-E. Qian, Ed. Chichester, U.K.: Wiley, 2016, pp. 215–222.

[62] T. Matsunaga *et al.*, "HISUI status toward 2020 launch," in *Proc. IEEE Int. Geosci. Remote Sens. Symp.*, Yokohama, Japan, 2019, pp. 4495–4498.

[63] M. Meini, A. Bini, L. Giunti, E. Fossati, and R. Formaro, "Hyperspectral payload for Italian PRISMA programme," in *Optical Payloads for Space Missions*, S.-E. Qian, Ed. Chichester, U.K.: Wiley, 2016, pp. 183–213.

[64] S. B. Mende *et al.*,, "Hadamard spectroscopy with a two-dimensional detecting array," *Appl. Opt.*, vol. 32, no. 34, pp. 7095–7105, 1993.

[65] P. Mouroulis, R. O. Green, and T. G. Chrien, "Design of pushbroom imaging spectrometers for optimum recovery of spectroscopic and spatial information," *Appl. Opt.*, vol. 39, no. 13, pp. 2210–2220, 2000.

[66] S. Murchie *et al.*, "Compact reconnaissance imaging spectrometer for mars (CRISM) on Mars reconnaissance orbiter (MRO)," *J. Geophys. Res.*, vol. 112, no. E5, pp. 1–57, 2007.

[67] B. S. Nakashima, G. A. Borstad, D. A. Hill, and R. C. Kerr, "Remote sensing of fish schools: Early results from a digital imaging spectrometer," in *Proc. IEEE 12th Can. Symp. Remote Sens. Geosci. Remote Sens. Symp.*, Vancouver, BC, Canada, 1989, vol. 4, pp. 2044–2046.

[68] NASA PACE Mission. 2013, Accessed: June 29, 2021. [Online]. Available: https://pace.oceansciences.org/home.htm

[69] R. A. Neville and I. Powell, "Design of SFSI: An imaging spectrometer in the SWIR," *Can. J. Remote Sens.*, vol. 18, no. 4, pp. 210–223, 1992.

[70] J. Nieke *et al.*, "The ocean and land colour imager (OLCI) for the sentinel 3 GMES mission: Status and first test results," *Proc. SPIE*, vol. 8528, 2012, Art. no. 85280C.

[71] J. Nieke *et al.*, "Ocean and land color imager on Sentinel-3," in *Optical Payloads for Space Missions*, S.-E. Qian, Ed. Chichester, U.K.: Wiley, 2016, pp. 223–245.

[72] J. Nieke and M. Rast, "Towards the copernicus hyperspectral imaging mission for the environment (CHIME)," in *Proc. IEEE Int. Geosci. Remote Sens. Symp.*, 2018, pp. 157–159.

[73] J. Nieke and M. Rast, "Status: Copernicus hyperspectral imaging mission for the environment (CHIME)," in *Proc. IEEE Int. Geosci. Remote Sens. Symp.*, 2019, pp. 4609–4611.

[74] L. J. Paxton, C.-I. Meng, D. E. Anderson, and G. J. Romick, "MSX—A multiuse space experiment," *Johns Hopkins APL Tech. Dig.*, vol. 17, no. 1, 1996, pp. 19–34.

[75] J. Pearlman, S. Carman, C. Segal, P. Jarecke, P. Barry, and W. Browne, "Overview of the Hyperion imaging spectrometer for the NASA EO-1 mission," in *Proc. IEEE Int. Geosci. Remote Sens. Symp.*, 2001, vol. 6, pp. 3504–3506.

[76] J. Pearlman, P. Barry, C. Segal, J. Shepanski, D. Beiso, and S. Carman, "Hyperion, a space-based imaging spectrometer," *IEEE Trans. Geosci. Remote Sens.*, vol. 41, no. 6, pp. 1160–1173, Jun. 2003.

[77] R. Perkins *et al.*, "Teledyne's multi-user system for earth sensing (MUSES)," in *Proc. Joint Agency Commercial Imagery Eval. Workshop*, Fort Worth, TX, USA, Apr. 11–15, 2016. [Online]. Available: https://calval.cr.usgs.gov/wordpress/wp- content/uploads/2016_JACIE-TDY_MUSES-3.pdf

[78] G. Piccioni *et al.*, "VIRTIS: The visible and infrared thermal imaging spectrometer," *ESA Special Publ.*, vol. 1295, pp. 1–27, 2007.

[79] W. M. Porter, T. G. Chrien, E. G. Hansen, and C. M Sarture, "Evolution of the airborne visible/infrared imaging spectrometer (AVIRIS) flight and ground data processing system," *Proc. SPIE*, vol. 1298, pp. 11–17, 1990.

[80] J. Praks *et al.*, "Aalto-1—An experimental nanosatellite for hyperspectral remote sensing," in *Proc. IEEE Int. Geosci. Remote Sens. Symp.*, 2011, pp. 4367–4370.

[81] J. Praks, A. Kestilä, T. Tikka, H. Leppinen, O. Khurshid, and M. Hallikainen, "AALTO-1 earth observation cubesat mission—Educational outcomes," in *Proc. IEEE Int. Geosci. Remote Sens. Symp.*, 2015, pp. 1340–1343.

[82] S.-E. Qian, *Optical Satellite Signal Processing and Enhancement*. Bellingham, WA, USA: SPIE Press, 2013.

[83] S.-E. Qian, Ed., "Review of spaceborne optical payloads," in *Optical Payloads for Space Missions*. Chichester, U.K.: Wiley, 2016, pp. 1–25.

[84] S.-E. Qian, *Hyperspectral Satellites and System Design*. Boca Raton, FL, USA: CRC Press/Taylor & Francis, 2020.

[85] R. Richter, "Atmospheric correction of DAIS hyperspectral image data," *Comput. Geosci.*, vol. 22, pp. 785−793, 1996.

[86] L. J. Rickard, R. Basedow, E. Zalewske, P. R. Silvergiate, and M. Landers, "HYDICE: An airborne system for hyperspectral imaging," *Proc. SPIE*, vol. 1937, pp. 173–179, 1993.

[87] A. Royer, N. T. O'Neill, D. Williams, P. Cliche, and R. Verreault, "Systeme de mesures de reflectances pour les spectrometres imageurs," in *Proc. IEEE 12th Can. Symp. Remote Sens. Geosci. Remote Sens. Symp.*, Vancouver, BC, Canada, 1989, vol. 4, pp. 2097–2100, 1:23–26.

[88] C. T. Russell *et al.*, "Dawn mission to Vesta and Ceres," *Earth Moon Planet*, vol. 101, pp. 65–91, 2007.

[89] C. M. Sarture *et al.*, "Airborne visible/infrared imaging spectrometer (AVIRIS): Sensor improvements for 1994 and 1995," in *Proc. 5th Annu. JPL Airborne Earth Sci. Workshop*, Jan. 23–26, 1995.

[90] A. Srivastava, User Interface Meeting 2016: "New Indian eye in GEO." Aug. 30, 2016. [Online]. Available: nrsc.gov.in

[91] S. D. Straight *et al.*, "Tactical satellite-3 mission overview and initial lessons learned," in *Proc. 24th Annu. AIAA/USU Conf. Small Satell.*, 2010.

[92] S. G. Ungar, J. S. Pearlman, J. A. Mendenhall, and D. Reuter, "Overview of the Earth Observing One (EO-1) mission," *IEEE Trans. Geosci. Remote Sens.*, vol. 41, no. 6, pp. 1149−1153, Jun. 2003.

[93] G. Vane and A. F. H. Goetz, "Terrestrial imaging spectroscopy," *Remote Sens. Environ.*, vol. 24, pp. 1–29, 1988.

[94] G. Vane *et al.*, "The airborne visible/infrared imaging spectrometer (AVIRIS)," *Remote Sens. Environ.*, vol. 44, pp. 127–143, 1993.

[95] A. A. Wagadarikar, M. E. Gehm, and D. J. Brady, "Performance comparison of aperture codes for multimodal, multiplex spectroscopy," *Appl. Opt.*, vol. 46, no. 22, pp. 4932–4942, 2007.

[96] A. A. Wagadarikar, N. P. Pitsianis, X. Sun, and D. J. Brady, "Video rate spectral imaging using a coded aperture snapshot spectral imager," *Opt. Exp.*, vol. 17, no. 8, pp. 6368–6388, 2009.

[97] J.-Y. Wang *et al.*, "Visible and near-infrared imaging spectrometer aboard Chinese Chang'E 3 spacecraft," in *Optical Payloads for Space Missions*, S.-E. Qian, Ed. Chichester, U.K.: Wiley, 2016, pp. 121–139.

[98] G. P. Weale, S. B. Achal, and C. D. Anger, "Application of CASI, a commercial remote-sensing instrument, to astronomy," *Proc. SPIE*, vol. 1235, 1990, pp. 799–800.

[99] R. E. Zee, "Space flight laboratory: Disruptively capable smaller satellites," in *Proc. Can. SmallSat Symp.*, Toronto, ON, Canada, Feb. 2–3, 2016.

[100] X. Zhao, Z. Q. Xiao, Q. Kang, Q. Li, and L. Fang, "Overview of the Fourier transform hyperspectral imager (HSI) boarded on HJ-1A satellite," in *Proc. IEEE Geosci. Remote Sens. Symp.*, 2010, pp. 4272–4274.

[101] M. Zucco, M. Pisani, and T. Cavaleri, "Fourier transform hyperspectral imaging for cultural heritage," in *Fourier Transforms: High-Tech Application and Current Trends*, G. S. Nikolic, M. D. Cakic, and D. J. Cvetkovic, Eds. London, U.K.: IntechOpen, 2017, doi: 10.5772/66107.
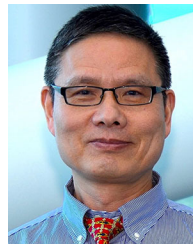
Shen-En Qian (Senior Member, IEEE) received the B.Eng. degree in industrial electrical automation from Anhui Polytechnic University in 1982, the M.S. degree in optoelectronics from Chinese Academy of Sciences in 1985, and the Ph.D. degree in telecommunication and electronic systems from Jilin University in 1990.

He continued his studies as a Postdoctoral Fellow with Observatoire de Meudon/CNRS, Paris, France, during 1992–1993 and as an NSERC Postdoctoral Visiting Fellow with Canadian Space Agency, Saint-Hubert, QC, Canada, from 1994 to 1996. From 1996 to 1998, he was an Associate Professor with the University of Quebec. Since 1998, he has been with the Canadian Space Agency. He is currently a Principal Scientist (top level) and Technical Lead of space missions. He is a scientific authority of Canadian government contracts and grants awarded to industry and academia in the development of space technologies and satellite missions. He heads an R&D team in the development of innovative space technology, satellite signal processing, and data applications for earth observation and deep space exploration. He is the sole author of four popular books on optical satellites, their system design, and signal processing published by SPIE Press, John Wiley, and CRC Press in USA and U.K. He also coauthored five other books. He holds 35 patents granted worldwide developed in Canadian government laboratories. He authored/coauthored more than 120 papers in the areas of optical spacecraft payloads, space technologies for satellite missions and deep space exploration, remote sensing, satellite signal processing and enhancement, and satellite data compression.

Dr. Qian is a Fellow of the Canadian Academy of Engineering, and a Fellow of the International Society of Optics and Photonics (SPIE). He is an Associate Editor of SPIE's *Journal of Applied Remote Sensing*, and an Associate Editor for the IEEE JOURNAL ON MINIATURIZATION FOR AIR AND SPACE SYSTEMS. He has delivered several IEEE webcasting lectures on innovative space technology and satellite signal processing to members in the world. He is an Adjunct Professor with York University. He was the recipient of the IEEE Canada Outstanding Engineer Award and Silver Medal in 2019. The Governor General of Canada presented him the Public Service Award of Excellence in the category of Scientific Contribution for his exceptional accomplishments in advancing Canadian space programs in 2016. He was also the recipient of the Canadian Government Invention Award for his multiple patents for space missions in 2004, and the Marie Curie Award from European Community in 1992.